BIOCHEMISTRY

Molecular basis of hUHRF1 allosteric activation for synergistic histone modification binding by PI5P

Papita Mandal[1]*, Karthik Eswara[1]†, Zhadyra Yerkesh[1]†, Vladlena Kharchenko[1]†, Levani Zandarashvili[2], Kacper Szczepski[1], Dalila Bensaddek[3], Łukasz Jaremko[1], Ben E. Black[2], Wolfgang Fischle[1]*

Chromatin marks are recognized by distinct binding modules, many of which are embedded in multidomain proteins. How the different functionalities of such complex chromatin modulators are regulated is often unclear. Here, we delineated the interplay of the H3 amino terminus– and K9me-binding activities of the multidomain hUHRF1 protein. We show that the phosphoinositide PI5P interacts simultaneously with two distant flexible linker regions connecting distinct domains of hUHRF1. The binding is dependent on both, the polar head group, and the acyl part of the phospholipid and induces a conformational rearrangement juxtaposing the H3 amino terminus and K9me3 recognition modules of the protein. In consequence, the two features of the H3 tail are bound in a multivalent, synergistic manner. Our work highlights a previously unidentified molecular function for PI5P outside of the context of lipid mono- or bilayers and establishes a molecular paradigm for the allosteric regulation of complex, multidomain chromatin modulators by small cellular molecules.

INTRODUCTION

Conformational flexibility and its control are a hallmark of biological regulation. Especially, intrinsically disordered regions allow proteins to explore a wide range of conformational space, enabling interaction with different partners and function in diverse contexts (*1*, *2*). Deterministic changes in protein conformation often occur in a regulated manner. Triggers for protein conformational change include differential splicing, posttranslational modification, and allosteric ligand binding. While the general importance of these regulatory modes has long been recognized, the exact molecular details of their working mechanisms are often unclear.

The specific recognition of chromatin modifications, i.e., DNA methylation and histone marks, is a hallmark of epigenetic regulatory processes. While many protein domains and folds have now been described to work in this context, their function and regulation in multidomain proteins and multiprotein complexes are still poorly understood. Allosteric regulation of such factors by small cellular metabolites is an intriguing possibility for fine-tuning chromatin-directed nuclear processes (*3*–*6*).

The role of lipid molecules as allosteric modulators has been primarily discussed in the context of lipid bilayers and membrane-bound proteins (*7*, *8*). However, recently, nuclear lipids associated with membraneless compartments or intranuclear speckles have been recognized as new signaling moieties (*9*). An interesting class of intranuclear lipids is phosphatidylinositol (PI) phosphates (phosphoinositides) that have emerged to play critical roles in different processes. For example, PIs serve as ligands for the NR5 orphan receptors to maximize their activity (*10*). Further, phosphatidylinositol 4,5-bisphosphate [PI(4,5)P_2] regulates binding of the BAF complexes to the nuclear scaffold and chromatin (*5*) and counteracts the transcriptional repressive function of histone H1 (*11*). The low abundant phosphatidylinositol-5-phosphate (PI5P) seems particularly important in controlling nuclear processes. Besides other effects, it has been reported to modulate ING2-mediated p53 acetylation and apoptosis (*12*), inhibit Cul3 E3 ligase activity (*13*), and alter TAF3-mediated transcription of specific genes (*3*). Overall, the different findings imply that nuclear PIPs interact with soluble chromatin factors in a manner that is different from membrane-bound proteins (*9*). However, the mechanistic details of how PIPs regulate the function of target factors are yet to be fully explored.

We have previously reported that the multidomain chromatin effector and writer protein UHRF1 [ubiquitin-like with plant homeodomain (PHD) and really interesting new gene (RING) finger domains 1] is an allosteric target of PI5P that modulates the chromatin engagement of different histone-binding domains of the factor (*14*). UHRF1 acts as a safeguard of the genome by maintaining global DNA methylation levels, protecting chromatin from DNA damaging agents, maintaining higher-order chromatin structures, and silencing repetitive DNA elements (*15*–*20*). UHRF1 is up-regulated in various types of malignancies, including breast, liver, and pancreatic cancer, where it plays a crucial role in promoting proliferation (*21*–*23*).

UHRF1 is composed of five domains that are connected through flexible linkers (Fig. 1A). The ubiquitin-like domain (UBL) directs ubiquitylation activity of UHRF1 toward histone H3 (*24*, *25*). A tandem tudor domain (TTD) and a plant homeodomain (PHD) recognize methylation at lysine 9 (K9me) and the unmodified N terminus of the histone H3 tail, respectively (*26*–*28*). The SET- and RING-associated (SRA) domain preferentially binds to hemimethylated (CpG) DNA (*29*, *30*), and the RING domain catalyzes H3 ubiquitination on K18 and/or K23 (*31*–*33*). While the functions of the individual domains of UHRF1 are well defined, their interplay is only emerging. Here, communication between the interdomain linker regions seems to be crucial (*14*, *34*–*37*). For example, hemimethylated

[1]Bioscience Program, Biological and Environmental Science and Engineering Division, King Abdullah University of Science and Technology (KAUST), Thuwal 23955, Kingdom of Saudi Arabia. [2]Department of Biochemistry and Biophysics, Penn Center for Genome Integrity, Epigenetics Institute, Perelman School of Medicine, University of Pennsylvania, Philadelphia, PA 19104, USA. [3]Core Laboratories, King Abdullah University of Science and Technology (KAUST), Thuwal 23955, Kingdom of Saudi Arabia.
*Corresponding author. Email: papita.mandal@kaust.edu.sa (P.M.); wolfgang.fischle@kaust.edu.sa (W.F.)
†These authors contributed equally to this work.

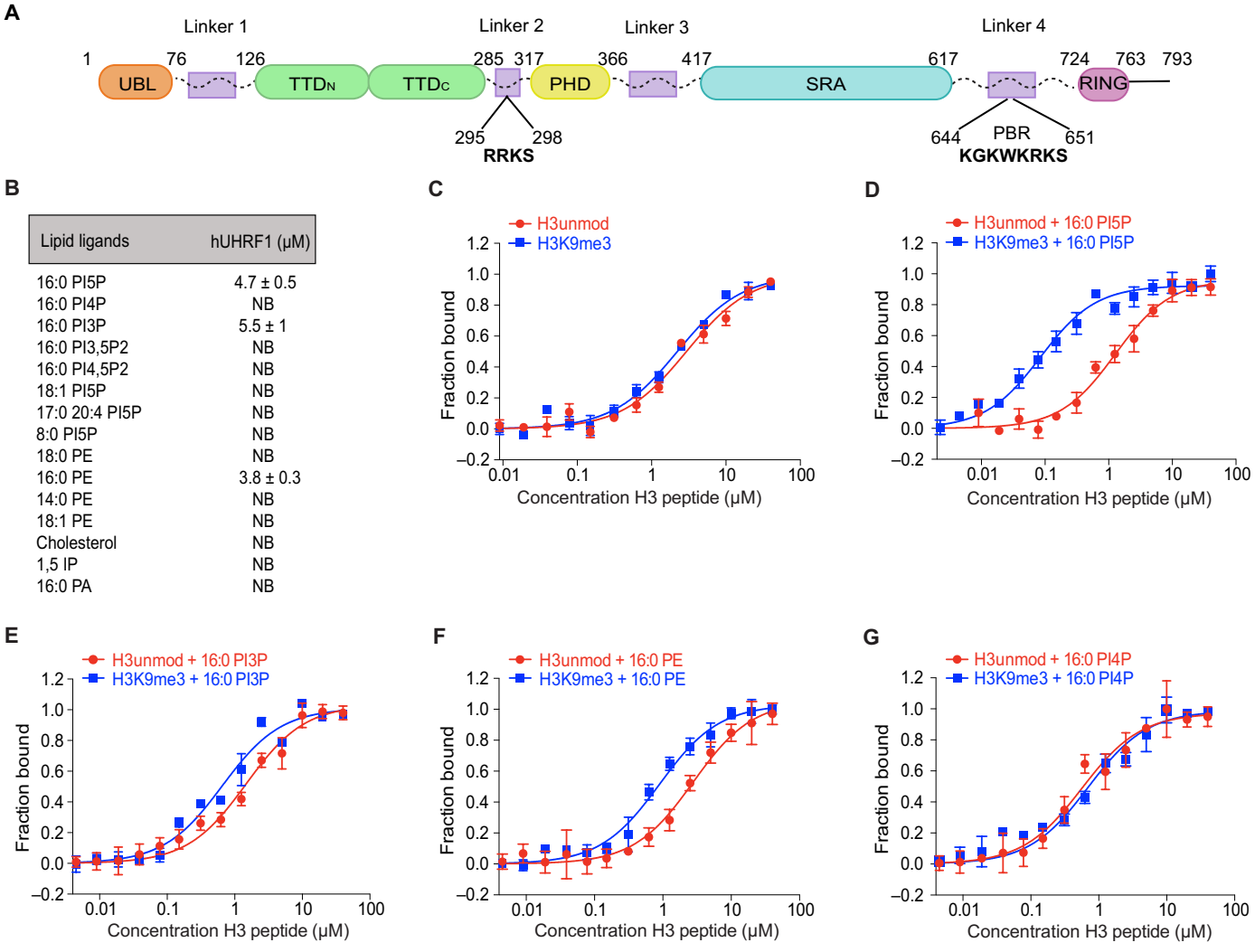

Lipid ligands	hUHRF1 (μM)
16:0 PI5P	4.7 ± 0.5
16:0 PI4P	NB
16:0 PI3P	5.5 ± 1
16:0 PI3,5P2	NB
16:0 PI4,5P2	NB
18:1 PI5P	NB
17:0 20:4 PI5P	NB
8:0 PI5P	NB
18:0 PE	NB
16:0 PE	3.8 ± 0.3
14:0 PE	NB
18:1 PE	NB
Cholesterol	NB
1,5 IP	NB
16:0 PA	NB

Fig. 1. hUHRF1 recognizes PIPs with a monophosphorylated inositol head group and di-C 16:0 acyl chains but gets activated only by PI5P. (**A**) Scheme illustrating the domain architecture of hUHRF1. UBL, ubiquitin-like domain; TTD, tandem tudor domain (TTDN-TTDC); PHD, plant homeodomain; SRA, SET and RING-associated domain; RING, really interesting new gene domain. Four putatively flexible linker regions connect the structured domains. PBR, polybasic region. Patches of amino acids relevant for this study are annotated. (**B**) Binding of hUHRF1 to phospholipids and other lipids of the indicated composition was analyzed by MST. Lipid ligands were titrated over a concentration range of 9 nM to 160 μM (for 16:0, 18:1, 18:0, 14:0, and 17:0 20:4 acyl chain lipids) and up to 1 mM (for 8:0 acyl chain lipid and the 1,5-IP head group). K_d deduced as average from three independent titration measurements is listed; error corresponds to SD; NB, not binding. (**C** to **G**) Titration series of H3 peptides (residues 1 to 20) of the indicated modification state with fluorescently labeled recombinant hUHRF1 were analyzed by MST in apo state (C) and in the presence of different phospholipids (D to G). $n = 3$; error bars: SD; K_d values are listed in table S1.

DNA triggers a not yet molecularly defined activation of UHRF1 that results in cooperation of the UBL and RING domains for enhanced H3 ubiquitylase function (*24*, *25*, *33*, *38*–*40*). Further, we have demonstrated that a polybasic region (PBR) in the linker 4 between SRA and RING domains can block TTD-H3K9me binding. Allosteric binding of PI5P releases the PBR from the TTD, enabling its H3K9me recognition (*14*). Other work unveiled that differential splicing in the flexible linker regions affects the overall regulation of human and mouse UHRF1 (*35*). The complex regulation of UHRF1 has made this factor an attractive model to study how a multidomain chromatin protein is conformationally and functionally controlled.

Here, we set out to delineate the molecular details of PI5P-mediated allosteric activation of human UHRF1 (hUHRF1). While hUHRF1 discriminates for the configuration of the phosphoinositide acyl chains, it binds different monophosphorylated inositol head groups (i.e., PI3P and PI5P). However, our biochemical and structural data show that only PI5P is functional in establishing a composite binding mode that bridges two interdomain linkers of hUHRF1. The resulting conformational rearrangement establishes multivalent, synergistic recognition of the isolated and nucleosome-embedded H3K9me tail by the TTD-PHD module. Our findings indicate a potential role of PI5P in targeting of hUHRF1 to H3K9me3 containing chromatin regions.

RESULTS

hUHRF1 recognizes the inositol head group and acyl chains of phosphoinositides

To better understand the molecular details of PI5P binding, we first determined the specificity of hUHRF1 for different phospholipids. In quantitative, in-solution measurements using microscale thermophoresis (MST), recombinant, full-length hUHRF1 (fig. S1A) displayed a strong preference for mono- versus bis (3,5 or 4,5)–phosphorylated inositol head groups, with only phosphoinositides carrying phosphorylation in the C3 [K_d(PI3P) = 5.5 μM] and C5 [K_d(PI5P) = 4.7 μM] positions showing interaction. Notably, the low micromolar binding to PI5P is right in the range of the predicted and indirectly measured nuclear concentration of this phosphoinositide (*41*, *42*). Only PI5P carrying the di-C16:0 but not the shorter di-C 8:0 or longer unsaturated 17:0,20:4 or di-C 18:1 acyl chain configurations bound hUHRF1 in these assays (Fig. 1B). Neither inositol 1,5-bisphosphate (1,5-IP) representing the isolated head group of PI5P nor di-C 16:0 phosphatidic acid (16:0 PA) representing the isolated tail group of PI5P was bound by hUHRF1. Of the different tested phospholipids, only the di-C 16:0 form of phosphatidylethanolamine (16:0 PE) but not its di-C 14:0, di-C 18:0, or the di-C 18:1 counterparts showed interaction. In addition, the unrelated lipid cholesterol was not bound by hUHRF1. Overall, the results indicated that hUHRF1 interacts with and discriminates the whole phosphoinositide molecule with specificity for the phosphorylation of the inositol head group and selectivity for the lengths and saturation level of the acyl chains.

PI5P specifically enhances hUHRF1 H3K9me3 binding

Next, we analyzed the effect of phosphoinositides on the interaction of hUHRF1 with the H3 tail by comparing binding affinities of the apo state (devoid of any ligand) versus phospholipid-bound state. We focused exclusively on the di-C 16:0 forms, as only these had shown notable interaction with the protein. As Fig. 1 (C and D) shows, PI5P only mildly (~2.6-fold) increased the binding strength of hUHRF1 to an unmodified H3-tail peptide [K_d(apo-hUhRF1) = 2.9 μM, K_d(hUHRF1(PI5P)) = 1.2 μM]. In contrast, interaction with a corresponding H3K9me3 peptide was increased up to 27-fold, with the PI5P-bound hUHRF1 displaying one of the strongest affinities to this modification observed for any factor (K_d = 0.08 μM) (see tables S1 to S3 for the full listing of K_ds determined in this study). On the contrary, PI3P and PE, which showed interaction with hUHRF1 comparable to PI5P, only induced a mild discriminatory effect on H3-tail recognition (Fig. 1, E and F). PI4P that did not interact with hUHRF1 in the direct binding studies did not have any effect on the binding to the H3 tail (Fig. 1G).

Previous reports have shown hemimethylated DNA and the UBL1-2 domain of USP7 influencing H3-tail binding of hUHRF1 (*36*, *40*, *43*). Compared to PI5P, we detected only mild enhancement (three- to fourfold difference) of hUHRF1 interaction with H3K9me3 in the presence of both these ligands (fig. S1, B and C, and table S1). On the basis of these analyses, we concluded that PI5P (di-C 16:0) is a unique and the most potent allosteric activator of hUHRF1 H3K9me3 binding.

PI5P directs multivalent, synergistic interaction of hUHRF1 with H3K9me3

To understand the differential peptide-binding modes of apo- and PI5P-bound hUHRF1, we performed hydrogen-deuterium exchange (HDX) mass spectrometry (MS) using recombinant hUHRF1. This method has been successfully used to demonstrate allosteric regulation of multidomain proteins by measuring the changes in backbone structure and dynamics (e.g., PARP1) (*44*, *45*). We compared the HDX pattern of the different forms of hUHRF1 in the absence and presence of unmodified and K9me3 H3 peptides. HDXMS experiments were performed over a time course of 10^1 to 10^4 s and revealed several partially overlapping peptides that were protected from deuterium uptake upon H3 peptide binding. For all experiments, almost no change in deuterium uptake was observed in regions outside of the TTD and PHD (Fig. 2A and figs. S2 to S4). In the apo state, the HDXMS patterns observed for hUHRF1 were highly similar for the unmodified and K9me3 H3 tails. The peptides with decreased deuterium exchange mapped in both cases primarily to a region of the PHD (region II, residues 313 to 357 amino acids) that according to three-dimensional (3D) structural studies interfaces directly with the N terminus of H3 (figs. S2B and S3B) (*27*, *28*). In contrast, peptides covering the TTD region showed similar deuterium exchange kinetics in the absence and presence of the unmodified and K9me3 H3 tails (Fig. 2, A to E). The results were consistent with the TTD of hUHRF1 not contributing to H3-tail binding in the absence of PI5P. Interaction in this state is solely mediated by the PHD.

In the PI5P-bound state, the unmodified H3 tail caused an HDXMS pattern like the apo state of hUHRF1, with peptides in the PHD but not the TTD region being protected from deuterium exchange (fig. S3A). In contrast, the K9me3 H3 tail caused significant decrease in deuterium uptake not only in the PHD (region II) but also in the TTD (region I) (Fig. 2, A and F to J, and fig. S2A). Peptides spanning the aromatic cage residues of the TTD (152 to 200 amino acids) were found to be protected. The findings implied that hUHRF1 recognizes the H3K9me3 mark specifically via the TTD domain in the PI5P-bound state.

Different reader domains of composite proteins or complexes can either work individually/independently (i.e., each domain having its separate ligand) or in combination with each other using a multivalent binding mode (i.e., different domains binding different functionalities of a singular ligand). The overall binding strength in multivalent binding can range from little more than additive (no coupling of the domains and no coupling of the functionalities of the multivalent ligand; increase in binding strength brought by kinetic rebinding/local concentration effects) to highly synergistic (reflecting strong coupling of the domains and functionalities of the multivalent ligand, "key and lock") (*35*, *46*). To determine whether the enhanced binding of hUHRF1 to H3K9me3 in the presence of PI5P is due to a multivalent and synergistic binding event, we measured H3 peptide-binding affinities of hUHRF1 after mutating either TTD or PHD and in the absence and presence of PI5P. Of importance for these experiments, neither the previously described TTD (TTD*: Y188A/Y191H) (*26*) nor PHD (PHD*: D334/D337A) (*47*) mutations had any effect on hUHRF1 PI5P binding (fig. S5A and table S2). While hUHRF1 PHD* in the apo state did not bind the unmodified or K9me3 H3 tail, interaction with the H3K9me3 peptide was observed in the PI5P-bound state (Fig. 2K). The results agreed with the TTD being blocked in the absence of PI5P and contributing to H3-tail binding in the presence of PI5P.

When analyzing hUHRF1 TTD*, this mutant recognized both unmodified (K_d = 5 μM) and K9me3 H3-tail peptides (K_d = 6.7 μM) with similar affinities, likely via the functional and free PHD

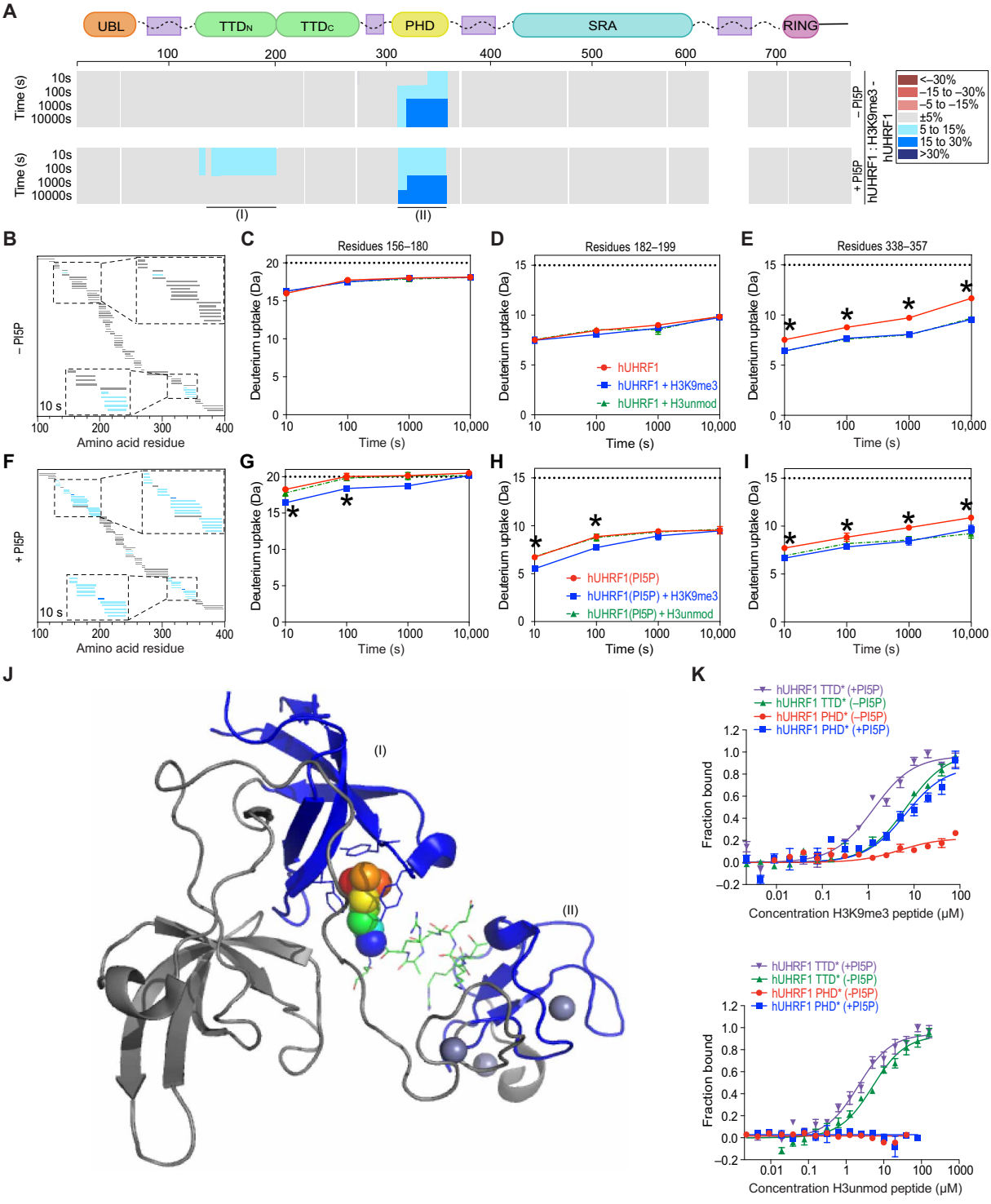

Fig. 2. PI5P directs multivalent, synergistic interaction of the hUHRF1 TTD-PHD module with H3K9me3. (**A**) The consensus at each amino acid position of the percentual difference of HDX at each time point is plotted with and without PI5P for each of ~200 unique partially overlapping peptides of the hUHRF1/H3K9me3 complex (fig. S2). White regions indicate gaps in the obtained peptide coverage of hUHRF1. Roman numerals indicate regions highlighted in (J). (**B**) Percentual difference in HDX upon binding to H3K9me3 peptide at 10s along the TTD-PHD region of hUHRF1. (**C** to **E**) HDX time curves of specific peptides encompassing the aromatic cage residues of TTD (C and D) and the N-terminal H3-tail–interacting residues in PHD (E) of apo-hUHRF1 binding to H3K9me3 peptide. Dashed line: peptide full-deuteration level; $n = 3$; asterisks: $P < 0.01$ (Student's t test); error bars: SD. (**F**) Same analysis as in (B) in the presence of PI5P. (**G** to **I**) Same analysis as in (C) to (E) in the presence of PI5P. (**J**) Crystal structure of the TTD-PHD module in complex with H3K9me3 peptide (4GY5). Regions undergoing differential HDX are numbered and highlighted in blue. The side chain of K9me3 is represented by multicolored spheres. (**K**) MST binding analyses; $n = 3$; error bars: SD; K_d values are listed in table S1.

domain. However, unlike the wild-type protein, this mutant showed only slight enhancement of interaction with the unmodified (K_d = 2.1 μM) and K9me3 (K_d = 1.3 μM) H3 peptides in the presence of PI5P. We note that the binding strength for H3K9me3 was significantly higher (K_d = 80 nM) for PI5P-bound, wild-type hUHRF1 (Fig. 1C and table S1) compared to the sum of the contribution of the individual TTD and PHD. Collectively, the findings pointed to PI5P binding establishing a TTD-PHD–dependent multivalent, synergistic recognition mode of hUHRF1 (Fig. 2J).

PBR/linker 4 is necessary but not sufficient for PI5P binding of hUHRF1

In previous work, we showed that PI5P binds to the PBR of hUHRF1. While this interaction unblocks the TTD from PBR-mediated inhibition (*14*), it cannot explain the observed multivalent, synergistic binding of H3K9me3 by hUHRF1 in the presence of PI5P. Additional changes in the protein that functionally couple TTD and PHD must occur. To uncover the molecular mechanism behind PI5P-driven enhanced H3K9me3 recognition, we first aimed to further characterize the PI5P binding of hUHRF1.

As shown previously (*14*), deletion of the C-terminal region (617 to 793 amino acids) of hUHRF1 caused complete loss of interaction with PI5P. Using a series of deletion constructs, we mapped the phospholipid-binding region to linker 4 (605 to 675 amino acids) that bound PI5P with a similar affinity as the intact protein (Fig. 3A). The binding specificity of this fragment was comparable to that of full-length hUHRF1 with strong preference for di-C 16:0 monophosphorylated phospholipids (fig. S5B).

To obtain further insights into the interaction of PI5P with linker 4, we used high-resolution multidimensional solution nuclear magnetic resonance (NMR) spectroscopy. Comparison of ^{1}H-^{13}C HSQC (heteronuclear single quantum coherence spectroscopy) spectra of linker 4 in the absence and presence of di-C 16:0 PI5P showed substantial chemical shift changes (Fig. 3B). To rule out that these chemical shift changes were unspecific and putatively caused by adding a phospholipid to the linker 4 polypeptide, we repeated the measurements using di-C 16:0 PI4P. No differences in the chemical shifts compared to linker 4 alone were observed (Fig. 3C). We fully assigned the linker 4 resonance peaks using a combination of 3D triple resonance ^{1}H-^{15}N–detected experiments (targeting backbone and side-chain resonances) and ^{1}H-^{13}C–detected 3D ^{13}C-edited nuclear Overhauser effect spectroscopy (NOESY) and (H)CCH total correlation spectroscopy (TOCSY) spectra (completing the side-chain assignments). The experiments identified two classes of linker 4 residues being selectively affected by PI5P and not by PI4P binding (Fig. 3B). The first class consists of amino acids with neutral or hydrophobic side chains, i.e., A614, A659, A638, T665, L612, and L615, and the second class encompasses positively charged residues. While in contrast to the well-resolved hydrophobic side chains containing methyl groups, we could not resolve all of the positively charged residues because of the severe overlap of the aliphatic ^{1}H-^{13}C correlations of lysine and arginine side chains, positively charged residues displayed considerable chemical shifts, and signal shape changes indicative of the interaction [Fig. 3B, see the Cδ/Hδ region of R649 overlapped with other arginines (zoomed on a small panel) and Cγ/Hγ region of the methyl groups of lysines on the main spectrum].

Solution-state structure determination of linker 4 in the PI5P-bound state by NMR was not possible because of the lipid-protein complex aggregating at the concentrations required for this analysis. We thus resorted to analyzing point mutants of linker 4 targeting the residues that showed chemical shift changes in the presence of the phosphoinositide. Besides mutation of the hydrophobic residues L612 and L615, mutation of the charged residues K644, K646, K648, and R649, but not K650, completely abolished interaction of linker 4 with PI5P (Fig. 3D). Other residues like A614 and A638 showed significant attenuation in interaction with the respective K_ds reduced by ca. 10-fold. We then set out to test these mutations in the context of full-length hUHRF1. To our surprise, none of the individual mutations that abolished the binding of PI5P to linker 4 had a similar effect in the context of the full-length protein. Mutation of the charged resides K644, K646, K648, and R649 had virtually no effect, while mutation of L615 and the double mutant L612/L615 showed some loss of interaction (three- and sixfold lower K_d compared to wild-type hUHRF1, respectively) (Fig. 3E and table S2). As only combination of mutation of multiple linker 4 residues (K644, K646, K646, and R649) completely abolished the binding of PI5P (we refer to this mutant as PBR*), we postulated that the binding modes of isolated linker 4 and full-length hUHRF1 for PI5P must be different and that additional binding interfaces must exist for this phospholipid in the full-length protein.

PI5P mediates interaction of hUHRF1 linkers 2 and 4

Multiple attempts to obtain x-ray crystals of full-length hUHRF1 in the absence and presence of PI5P failed. It also turned out impossible to analyze hUHRF1/PI5P binding in detail using NMR because of the high concentrations of protein and, in particular, phospholipid required for this method. We therefore turned to HDXMS, which requires comparatively less concentrated hUHRF1/PI5P complex, to obtain structural insights into this interaction. In the initial analysis, we compared the HDX pattern of PI5P-bound hUHRF1 with the protein in the apo state. Although we did not get full coverage for the PBR and surrounding regions, we noticed strong protection from deuterium uptake in peptides covering linker 4 and a region immediately upstream corresponding to the C terminus of the SRA domain (580 to 605 amino acids) (fig. S6). However, a low level of protection was observed throughout the protein, and we were unable to map any other regions affected by PI5P. We reasoned that the presence of a lipid moiety is putatively causing desolvation of the protein during HDX and thereby masking HDX patterns caused by PI5P binding. To map out such background effects generally caused by the presence of a phospholipid in the reactions, we took advantage of the interaction of hUHRF1 with di-C 16:0 PI3P. PI3P interacts with the isolated linker 4 and full-length hUHRF1 but does not enhance hUHRF1 H3K9me3 binding (Fig. 1 and fig. S5B). Thus, comparing the HDX patterns of the PI5P bound protein with those of the PI3P-bound protein should allow further mapping of the molecular consequences of hUHRF1 PI5P binding for the conformation of the protein.

HDXMS experiments were performed over a time course of 10^{1} to 10^{5} s (Fig. 4A and fig. S7). As predicted, the linker 4 and C-terminal region of the SRA did not show differential protection in the analysis, because both PI5P and PI3P interact with these regions. We observed significant decrease in HDX in the TTD domain (127 to 151 amino acids; region I), in linker 2 (274 to 312 amino acids; region II), and in the PHD domain (319 to 340 amino acids; region III) (Fig. 4, A to D and F, and fig. S7). These regions either participate directly in PI5P binding and/or undergo conformational rearrangements that minimize their deuterium uptake.

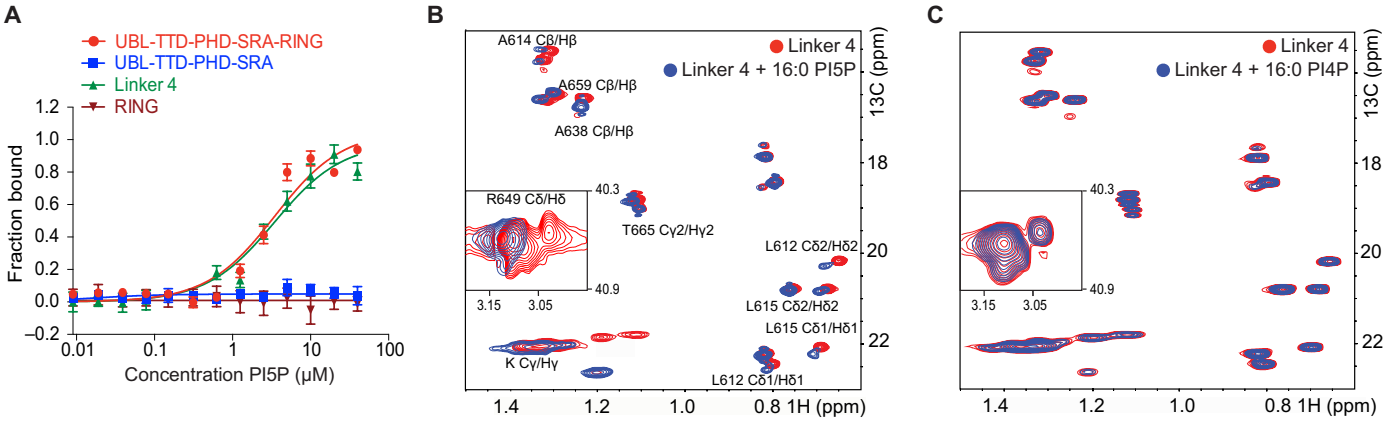

D

Linker 4	16:0 PI5P (μM)
WT	3.4 ± 0.7
Y611*	10.5 ± 2
L612*	NB
A614*	32.5 ± 2
L615*	NB
F637*	7.2 ± 1
A638*	36.7 ± 3
K644*	NB
G645*	10.4 ± 1
K646*	NB
W647*	15.1 ± 1
K648*	NB
R649*	NB
K650*	3.9 ± 0.6
A652*	13.7 ± 2

E

hUHRF1	16:0 PI5P (μM)
WT	3.4 ± 0.9
PBR*	NB
K644*	5.4 ± 0.6
K646*	2.9 ± 0.3
K648*	4.1 ± 0.4
R649*	2.6 ± 0.3
A614*	5.8 ± 0.6
L615*	10.3 ± 1.7
L612/L615*	21.9 ± 0.7
A638*	5.2 ± 0.3

Fig. 3. The PI5P binding mode of PBR/linker 4 is different from full-length hUHRF1. (**A**) Titration series of di-C 16:0 PI5P with fluorescently labeled, recombinant, full-length, and truncated hUHRF1 analyzed by MST. $n = 3$; error bars: SD; K_d values are listed in table S2. (**B** and **C**) Solution NMR spectra (2D ^{1}H-^{13}C HSQC-CT, constant time) of hUHRF1 linker 4 (residues 605 to 675) in the absence and presence of di-C 16:0 PI5P (B) and di-C 16:0 PI4P (C). Amino acids that showed changes in chemical shift upon PI5P binding are indicated by residue number/type. The overlapped signals of the aliphatic $^{1}H/^{13}C$ correlations of lysine and arginine (enlarged in the inset) side chains are shown in (B). (**D** and **E**) K_d for di-C 16:0 PI5P binding of wild-type and point mutated recombinant linker 4 (D) and full-length hUHRF1 (E) as determined by MST. Mutations showing significant effects are highlighted. Single and double mutations: residues Y611, L612, A614, L615, A638, G645, W647, and A652 were mutated to R; residues F637, K644, K646, K648, R649, K650, and S651 were mutated to A. PBR*: K644A, K646A, K648A, R649A, K650A, and S651A. Results represent averages of minimally three independent experiments. NB, not binding; error represents SD.

Region I maps to the TTD surface groove (a.k.a. acidic patch or R pocket) (*14*, *35*) that shares binding interface with either linker 4/PBR (*14*, *36*) or linker 2 (*47*). Like linker 4, linker 2 is enriched in positively charged amino acids (RRK motifs; see Fig. 1). Among these residues, R296 is crucial for interaction with the TTD surface groove (*47*). For hUHRF1(PI5P), the peptides in the TTD surface groove showed 100 times delay, achieving the same level of deuteration as observed for hUHRF1(PI3P) (Fig. 4B). The HDX profile of linker 2 (region II) indicated induction of more protection from deuterium exchange in linker 2 in the presence of PI5P compared to PI3P (Fig. 4C and fig. S9). Region III identified in the analysis maps to the binding site of the N terminus of the H3 tail (*27*, *28*). The corresponding peptides showed slow HDX compared to the control set throughout the time course (Fig. 4D), indicating that this region is stably locked in a state facing the TTD–linker 2.

Peptides that map to the SRA domain (476 to 512 amino acids; region IV) showed higher deuteration levels when comparing hUHRF1(PI5P) with hUHRF1(PI3P), suggesting that this region gets exposed to the surroundings because of conformational rearrangement caused by PI5P binding (Fig. 4, A, E, and F, and fig. S7). The HDX patterns were consistent with half of this region forming loop structures and the other half acquiring stable secondary structures in the presence of PI5P. In contrast, in the state of hUHRF1(PI3P), the number of loop residues is decreased, and the region assumes a relatively stable secondary structure (Fig. 4E).

To evaluate whether slow/less deuteration in the identified regions of hUHRF1 is caused by direct interaction with PI5P, we analyzed binding of the phospholipid to isolated linker 2, TTD, and PHD. In MST experiments, none of these regions showed any interaction with PI5P, indicating that other parts of the protein such as linker 4 are required for eliciting the observed effects (Fig. 4G). Next, we tested interaction of these regions with PI5P in the presence of linker 4. PI3P served as control in these experiments. In line with our earlier work (*14*), we found that the TTD interacted with the apo–linker 4 but that this interaction was lost in the presence of PI5P (fig. S10A). In contrast, no interaction of the PHD domain with linker 4 was detected in the presence or absence of PI5P (fig. S10B). The results suggested that the protection observed in HDXMS is most likely due to conformational rearrangements of hUHRF1 induced by PI5P binding.

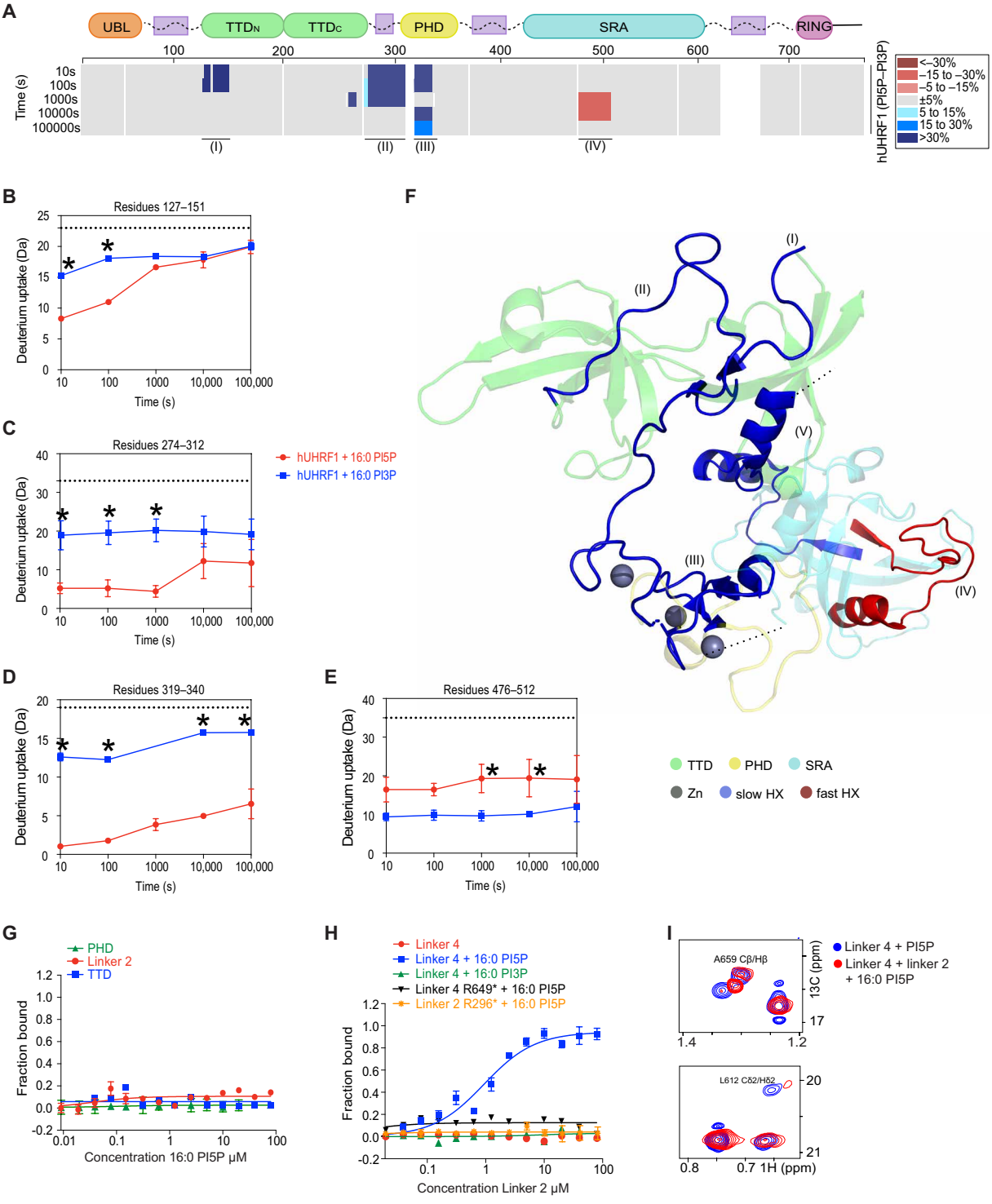

Fig. 4. PI5P is a conformation-specific allosteric activator of hUHRF1. (**A**) The consensus at each amino acid position of the percentual difference of HDX at each time point is plotted with and without PI5P for each of ~200 unique partially overlapping peptides of hUHRF1. White regions indicate gaps in the obtained peptide coverage of hUHRF1. Roman numerals indicate regions highlighted in the PDB structure in (F). (**B** to **E**) HDX time curves of specific peptides encompassing TTD surface groove (B), linker 2 (C), H3-tail–interacting interface of PHD (D) and the DNA-binding region of SRA (E). Dashed line: peptide full-deuteration level; $n = 3$; asterisks: $P < 0.01$ (Student's *t* test); error bars: SD. (**F**) Combined structural model of the TTD-PHD module (4GY5) and the SRA domain (3CLZ) of hUHRF1. Blue (I, II, and III): regions of slow HDX. Red (IV): region of fast HDX. Region (V) is highlighted in blue based on slow HDX as shown in fig. S6. Dotted lines, arbitrary continuation of the structure. (**G** and **H**) MST binding analyses; $n = 3$; error bars: SD. K_d values are listed in table S1. (**I**) Solution NMR spectra of hUHRF1 linker 4 together with di-C 16:0 PI5P in the absence (blue) and presence (red) of linker 2.

Using isolated peptides in MST and in affinity pull-down assays, we found that linker 2 interacted with linker 4 in the presence of PI5P but not in its absence (Fig. 4H and fig. S10C). This effect was highly specific, because PI3P that can bind linker 4 (Fig. 4H and fig. S5B) did not have a similar effect. Mutagenesis of R649 in linker 4 that is implied in PI5P binding abolished the interaction with linker 2. Similarly, mutagenesis of R296 within linker 2 caused loss of PI5P-mediated binding of linker 4. To further validate interaction of linkers 4 and 2 in the presence of PI5P, we performed ^{1}H-^{13}C HSQC NMR spectroscopy. When comparing spectra of linker 4(PI5P) in the absence and presence of linker 2 (Fig. 4I and fig. S10, D and E), additional chemical shift changes in residue A659 and loss of intensity of residue L612 were observed (Fig. 4I).

PI5P directs synergism of hUHRF1 TTD-PHD in H3K9me binding

To further understand the allosteric regulation of hUHRF1 by PI5P, we analyzed phosphoinositide binding of a series of different mutants of the full-length protein and monitored the TTD-PHD–dependent synergism by measuring their H3-tail binding behavior in the apo- versus PI5P-bound state. In the apo state, the PBR* mutant of multiple charged residues showed only fourfold enhancement for H3K9me3 binding compared to the wild-type protein (Fig. 5A). This finding was consistent with this mutant adopting a "TTD open" state by releasing linker 4 from the TTD surface groove. No further enhancement of the interaction with H3K9me3 was seen in the presence of PI5P, which agrees with this mutant not interacting with PI5P (Fig. 3E). The results further confirmed that TTD unblocking alone is not sufficient for establishing a multivalent, synergistic H3K9me3-binding mode of hUHRF1.

Although the R296* and R649* mutations abolished interaction with PI5P in isolated linkers 2 and 4, these mutations had no effect on PI5P binding in the context of the full-length protein [K_d(R296*) = 5 μM, K_d(R649*) = 3 μM], probably due to a mutation buffering effect (Fig. 5B and table S2) (*48*). While the R649* mutation similar to the PBR* mutations unblocked the TTD inhibition, the unaffected PI5P binding activated multivalent, synergistic H3K9me3 interaction of hUHRF1 with a binding strength similar to the wild-type protein (K_d = 67 nM; Fig. 5C and table S1). In contrast, the R296* mutation showed no signs of TTD unblocking with its binding to H3K9me3 like wild-type apo-hUHRF1 (K_d = 8.9 μM; Fig. 5C). While PI5P increased the interaction of this mutant with H3K9me3, the effect was significantly lower compared to the wild-type protein (K_d = 0.4 μM; Fig. 5C). As the enhancement of binding was comparable to that of the R649* mutation in the absence of PI5P, we deduced that the observed effect is due to the PI5P-mediated release of linker 4 from the TTD. However, as linker 2 R296* cannot access the TTD surface groove, no synergism between TTD and PHD is established.

To further test the hypothesis that PI5P induces TTD-PHD synergism via positioning linker 2 in the surface groove of the TTD, we analyzed the D142* mutation that disrupts both linker 2 and linker 4 interactions with the TTD (i.e., the TTD is neither blocked by PBR/linker 4 nor activated by linker 2) (*14*, *36*, *47*). hUHRF1 D142* showed an almost 20-fold weaker interaction with PI5P compared to the wild-type protein (K_d = 60 μM; Fig. 5B). The

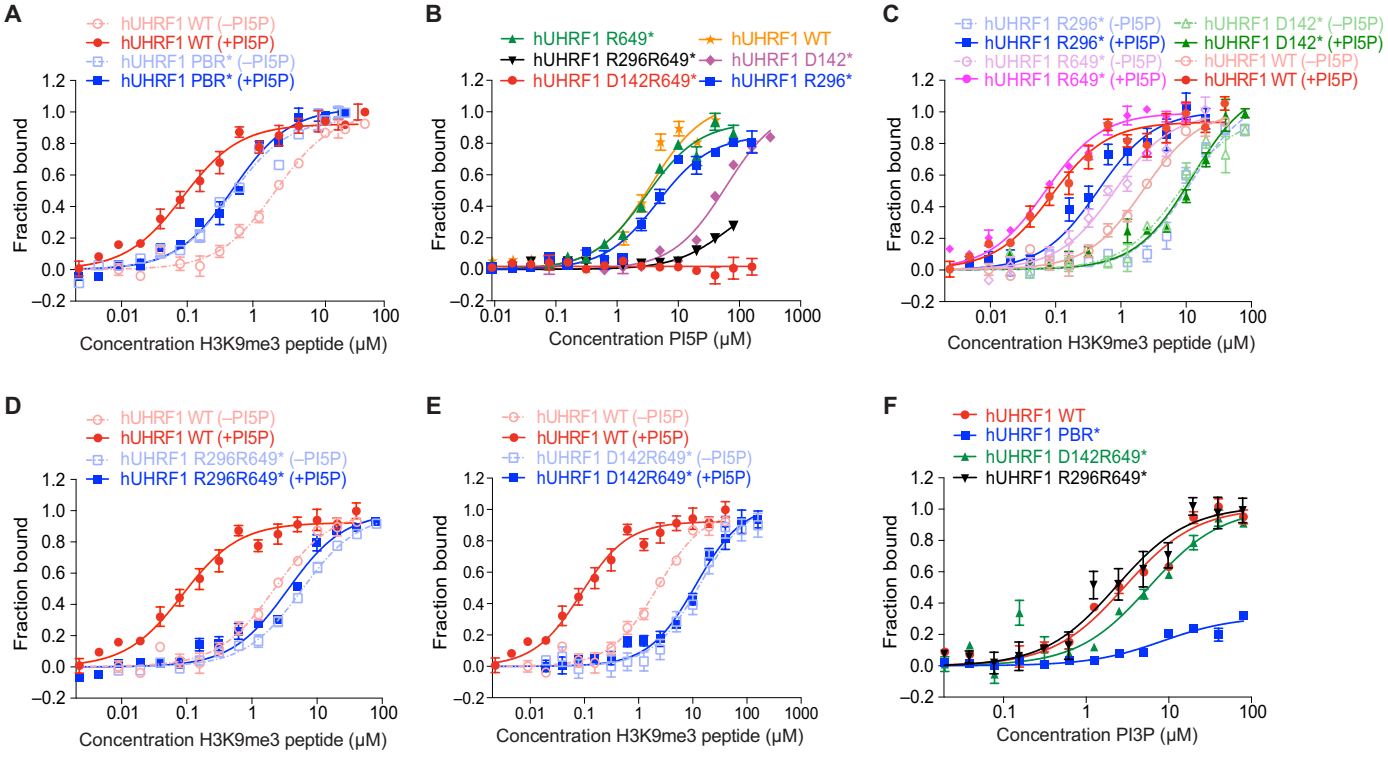

Fig. 5. PI5P directs synergism of hUHRF1 TTD-PHD in H3K9me binding. (**A** to **F**) Titration series of H3K9me3 peptide (in the absence and presence of di-C 16:0 PI5P), PI5P, or PI3P with fluorescently labeled, mutant, and wild-type, full-length hUHRF1 were analyzed by MST. PBR*: K644A, K646A, K648A, R649A, K650A, S651A; R296*: R296A; R649*: R649A; D142*: D142A; R296R649*: R296A, R649A; and D142R649*: D142A, R649A. n = 3; error bars: SD; K_d values are listed in tables S1 and S2.

results clearly implied that hUHRF1 must undergo 3D rearrangements to acquire the PI5P-binding compatible state. As expected, hUHRF1 D142* did not show any enhancement for H3K9me3 binding upon PI5P addition (Fig. 5C). To recapitulate a similar inactive state as D142*, we analyzed the R296R649* linker 2 and linker 4 double mutant and the TTD surface groove and linker 4 double mutant D142R649*. Like D142*, these double mutants disrupt linker 2 and linker 4 interaction with the TTD surface groove. Both mutants did not bind to PI5P (Fig. 5B), and addition of the phospholipid did not enhance hUHRF1 H3K9me3 binding further (Fig. 5, D and E).

We also assessed the specificity of the allosteric interaction and conformational activation of hUHRF1 by measuring PI3P binding to the mutant proteins. PI3P binding to hUHRF1 was only disrupted by the PBR* but not the R296R649* and D142R649* mutations, indicating that PI5P but not PI3P is bound by an interface generated between TTD, linker 2, and linker 4 (Fig. 5F). Overall, the results verified that conformational rearrangements of hUHRF1 are necessary for both PI5P interaction and induction of a multivalent, synergistic H3K9me3 binding mode.

PI5P enhances hUHRF1 H3K9me3 binding in the nucleosomal context

To investigate the physiological relevance of the hUHRF1 allosteric regulation, we performed pull-down assays of immobilized recombinant H3unmodified and H3K9me3 nucleosomes with recombinant hUHRF1 (Fig. 6, A to C, and fig. S11, A and B). In the absence of PI5P, hUHRF1 did not show any preference for H3unmodified or H3K9me3 nucleosomes (Fig. 6, A and C). However, in the same assay, hUHRF1 from HeLa nuclear extract displayed specificity for the modified nucleosomes (fig. S11C). Adding PI5P to recombinant hUHRF1 recuperated this observation with the protein showing approximately fivefold more enrichment on H3K9me3 nucleosomes compared to the unmodified counterpart (Fig. 6, A and C). To test whether PI5P in this context directs a synergistic binding mode of hUHRF1, we analyzed the D142R649* mutant protein that uncouples PI5P and H3K9me3 binding (Fig. 5, B and E). hUHRF1 D142R649* bound H3unmodified and H3K9me3 nucleosomes equally and irrespective of PI5P addition (Fig. 6B). We did not detect any effect of PI4P onto hUHRF1 nucleosome binding, verifying the specificity of the PI5P effect (Fig. 6, A and C).

To further validate the effect of PI5P onto the binding of hUHRF1 to H3K9me3 nucleosomes, we performed electrophoretic mobility shift assays (EMSAs). In this assay, hUHRF1 in the absence of PI5P showed slight preference for H3K9me3 nucleosomes (apparent K_d = 0.6 μM) compared to H3unmodified nucleosomes (K_d = 1.1 μM) (Fig. 6D, fig. S11, D and E, and table S3). The presence of PI5P significantly increased the binding affinity of hUHRF1 for H3K9me3 nucleosomes (K_d = 0.2 μM), while PI4P did not show any effect. Both PI5P and PI4P showed a similar increase in binding to the H3unmodified nucleosomes, indicating a nonspecific effect of the phospholipids. The results agree with PI5P allosterically regulating interaction of hUHRF1 with the HK9me3 mark within nucleosomes, albeit to a lesser degree than with the isolated H3 tail.

DISCUSSION

We are reporting the molecular details of allosteric regulation of a chromatin reader protein by a phosphoinositide. Using quantitative biophysical methods and structural analysis, we obtained detailed insights into the conformational changes induced in hUHRF1 upon interaction with PI5P that bring together different, distant regions of the protein. Our findings contrast and expand earlier work investigating isolated modules of hUHRF1 that, while describing independent interaction modes, did not reflect the regulation and multivalent, synergistic H3K9me3-binding functionality of the whole protein (*37*, *49*). We think the PI5P-induced transitions of hUHRF1 occur in two steps: from a TTD-blocked ground state through a TTD-open intermediate state to a TTD-PHD synergistic activated state.

In the ground state, the PBR/linker 4 is bound to the peptide-binding groove of the TTD (Fig. 6E(i)). R649 of linker 4 is positioned into the R-pocket and especially interacts with residues D142 and E153 of the TTD surface (*14*, *50*). Other PBR residues (K648 and S651) also connect with the TTD surface, strengthening the interaction. Last, P656 of linker 4 gets stably positioned into the aromatic cage of the TTD (Y191, F152, and Y188) that is required for K9me3 binding (*50*). As consequence, the TTD surface is blocked for both interaction with linker 2 and the H3 N-terminal tail.

The intermediate state of hUHRF1 is characterized by removal of the PBR/linker 4 from the TTD surface. Experimentally, it is obtained by PBR mutagenesis (PBR*) or binding to PI3P. In this state, linker 2 can access the TTD surface groove (Fig. 6E(iii)). However, there is no stable association, and linker 2 positions fluctuate (Fig. 6E (iv)). Structural studies of isolated TTD-PHD have indeed shown that this dual module can adopt either a compact or extended confirmation depending on the position of linker 2 (*37*, *49*, *51*). H3K9me3 binding either independently by the TTD (linker 2 not bound by the TTD surface groove) or synergistically by the TTD and PHD (linker 2 positioned in the surface groove) is possible but not enforced in this state. In consequence, the intermediate state shows a slight preference for H3K9me3 over the unmodified H3 tail.

The activated state is characterized by synergism between the TTD and PHD domains (Fig. 6E(ii)). di-C 16:0 PI5P but not PI3P binding drives large conformational rearrangements that not only free the TTD from PBR/linker 4 inhibition but also stabilizes the orientation of the PHD domain by firmly positioning linker 2 on the TTD surface groove. This is accomplished by a composite interaction of linkers 4 and 2 with PI5P that is not possible with the related PI3P. Mutagenesis of the TTD surface groove indicates that linker 2 must be on the TTD surface to be able to bind PI5P and to form a complex with PI5P-bound linker 4 (Figs. 4H and 5, B and E). Because of a favorable and stable orientation and distance of the TTD and PHD, multivalent, synergistic binding of H3K9me3 with the N terminus of H3 bound by the PHD and the K9me3 moiety inserted into the aromatic cage of the TTD is enabled.

Besides the changes in TTD, linker 2, and linker 4, PI5P binding also affects the PHD and a region of the SRA domain (476 to 512 amino acids) that specifically recognizes methyldeoxycytosine bases in double-stranded DNA (Fig. 4) (*28*, *29*). Previous studies on isolated domains have shown that the SRA can bind to the PHD and partially inhibit its interaction with the unmodified N terminus of the H3 tail (*35*). We think that because of the PI5P-driven overall conformational rearrangements, the SRA-PHD interaction opens, which aids slight enhancement in unmodified H3-tail recognition (Figs. 1D and 2K, bottom).

While the effect of PI5P onto hUHRF1 K9me3 binding is very strong on the free H3 tail, it is somewhat dampened in the context of nucleosomes. Some of the observed difference can be attributed to technical aspects, as we could not titrate PI5P to the same saturation

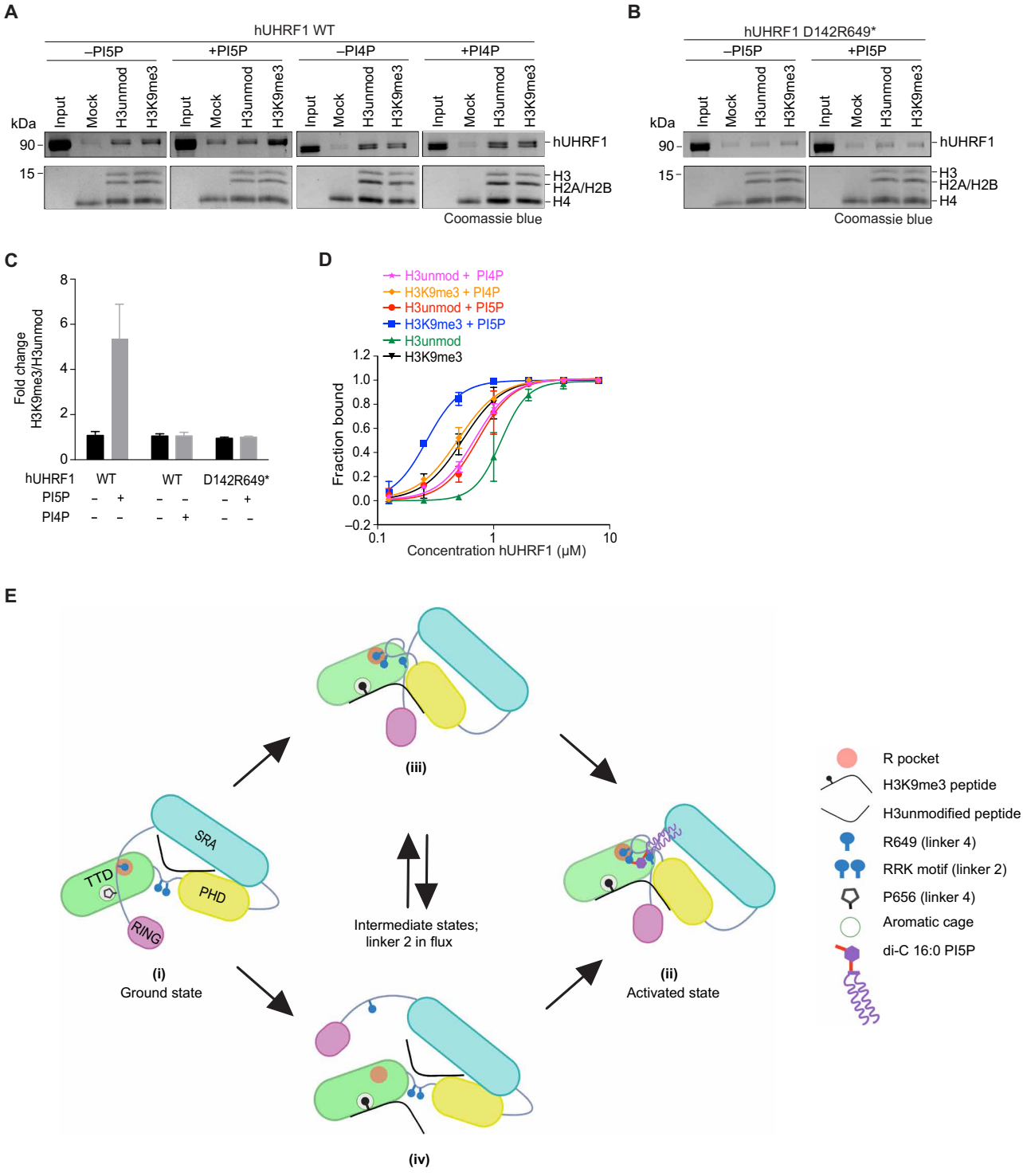

Fig. 6. PI5P enhances interaction of hUHRF1 with H3K9me3 nucleosomes. (**A**) Recombinant, H3unmodified, or H3K9me3 nucleosomes were used in pull-down experiments with recombinant hUHRF1 in the absence or presence of PI5P or PI4P. The recovered material was run on SDS–polyacrylamide gel electrophoresis and stained with Coomassie blue. Running positions of molecular weight markers, histone proteins, and hUHRF1 are indicated. Mock, control pull down with streptavidin beads only; input corresponds to 2%. (**B**) Analysis as in (A) but using recombinant D142A, R649A mutated hUHRF1 (D142R649*) protein. (**C**) Quantification of the experiments in (A) and (B). Data are plotted as average fold change (hUHRF1 enrichment on H3K9me3 nucleosome versus H3unmodified nucleosome). $n = 3$; error bars: SD. (**D**) Titration series of recombinant hUHRF1 with H3unmodified and H3K9me3 recombinant nucleosomes in the absence and presence of PI5P or PI4P were analyzed by EMSAs. $n = 3$; error bars: SD. (**E**) Putative conformational states of wild-type and mutant hUHRF1 proteins and their induced transition by PI5P. For details, see main text, Discussion section.

levels of hUHRF1 in these experiments as compared to the measurements with free peptides. On a biochemical level, it was shown earlier that the SRA domain of the protein has general DNA binding activity (*52*). This property might, besides general electrostatic effects limiting the availability of the nucleosomal H3 tail and, in particular, in the absence of linker histones (*53*), contribute to the observed differences. The main role of the SRA is, however, in the recognition of hemimethylated DNA that triggers activation of the ubiquitin E3 ligase activity of the RING domain of hUHRF1 via an unknown mechanism (*40*). Because we did not observe an effect of PI5P binding onto the interaction of hUHRF1 with hemimethylated DNA (fig. S12A), it is tempting to speculate that the PI5P and hemimethylated DNA-dependent conformations of the protein are exclusive to each other, thereby determining distinct functionalities of the protein.

Recent studies suggested that interaction of hUHRF1 with a methylation mark in DNA ligase 1 (LIG1) promotes its recruitment to sites of DNA replication (*54*). On the basis of domain studies, it was implied that this interaction is solely dependent on the TTD, as LIG1 is missing the residues corresponding to the N terminus of H3, which drive interaction with the PHD (*55*). We found the apo state of hUHRF1 to show very limited interaction with LIG1 methylated on the K126 site. This interaction was, however, strongly enhanced in the hUHRF1 PI5P-bound state (K_d = 0.5 μM; fig. S12B), indicating the potential role of PI5P in chromatin targeting of hUHRF1via nonhistone methylated chromatin binders.

In the absence of detailed structural insights on the hUHRF1(PI5P) complex, it is unclear in what physical state PI5P interacts with hUHRF1. Phospholipids are amphiphilic molecules that tend to form bicelles in aqueous solvent depending on the properties of the acyl chains. Binding analysis using PI5P bicelles (PI5P/DMPC/DHPC or PI5P/DHPC bicelles) versus free PI5P showed that hUHRF1 prefers the nonbicelle state of PI5P (fig. S12, C and D). Further considering the specificity (for the head group) and selectivity (for the acyl chain) for di-C 16:0 PI5P (Fig. 1B) and the effects of charge and hydrophobic properties changing mutations on PI5P binding (Fig. 3E), it seems likely that hUHRF1 recognizes individual molecule(s) of PI5P by interacting simultaneously with the head group and the acyl chains of the phospholipid.

Our finding that hUHRF1 is regulated by di-C 16:0 PI5P raises the question whether it is a signaling molecule or a structural cofactor. Previous efforts to purify PI5P-bound hUHRF1 from nuclear extract were unsuccessful, likely indicating that PI5P acts as a signaling molecule and its association with hUHRF1 is a regulated event (*14*). The nuclear concentration of PI5P has been shown to be influenced by different external and internal stimuli such as stress response (*56*–*59*) and the cell cycle (*60*, *61*).

While our study revealed the molecular details of PI5P-mediated allosteric control of hUHRF1, defining the physiological role of such regulation events remains a major challenge. hUHRF1 interacts with several factors associated with the DNA damage response such as Eme1, TIP60, Ku70, and PARP1 (*62*–*64*). Because H3K9me3 has an important role in repair mechanisms of DNA damage (*65*), we speculate that hUHRF1 might recruit repair factors to H3K9me3-enriched heterochromatic loci, which are otherwise inaccessible (*34*). In addition, recent work revealed the involvement of hUHRF1 in the replication-coupled and replication-uncoupled pathways of DNA maintenance methylation. While DNMT1-PCNA and hUHRF1-LIG1 interaction might govern replication-coupled maintenance, interaction between hUHRF1 and methylated H3K9 seems to play a pivotal role in the replication-uncoupled pathway (*66*). Thus, PI5P binding might modulate the replication-uncoupled DNA maintenance methylation machinery by regulating the interaction of hUHRF1 with H3K9me3. The enzyme systems and putative signaling events that specifically control nuclear PI5P are complex and difficult to manipulate experimentally (*60*, *61*, *67*). Furthermore, there are no methods for targeted manipulation of a specific PI5P species, such as di-C 16:0 PI5P. Chemical biology approaches for derivatizing PI5P (*68*) and nuclear injection (*69*, *70*) coupled to single-cell analysis might be promising avenues in this regard to deduce the functional role of hUHRF1 regulation by PI5P.

MATERIALS AND METHODS

Plasmids

All cloning was done using human UHRF1 cDNA (NM_001048201) and following standard procedures. For bacterial expression of recombinant proteins, the following constructs were used: pETM13 hUHRF1 (amino acids 1 to 793)–6xHis, pETM13 linker 4 (amino acids 605 to 675)–6xHis, pETM13 RING (amino acids 675 to 793)–6xHis, pETM13 UBL-TTD-PHD-SRA (amino acids 1 to 619)–6xHis, pET16b 10xHis-TEV-TTD (amino acids 126 to 285), pETM13 PHD (amino acids 301 to 376)–6xHis, and pET16b 10xHis-TEV-USP7 UBL1-2 (amino acids 560 to 792). Point mutagenesis was performed following the QuickChange Protocol (Stratagene).

Lipids

Phosphatidylinositol 5-phosphate diC16 (di-C 16:0 PI5P; Echelon, #P5016), phosphatidylinositol 4-phosphate diC16 (di-C 16:0 PI4P; Echelon, #P4016), phosphatidylinositol 3-phosphate diC16 (di-C 16:0 PI3P; Echelon, #P3016), phosphatidylinositol 4,5-bisphosphate diC16 [di-C 16:0 PI(4,5)P2; Echelon, #P4516], phosphatidylinositol 3,5-bisphosphate diC16 [di-C 16:0 PI(3,5)P2; Echelon, #P3516], phosphatidylinositol 5-phosphate diC8 (di-C 8:0 PI5P; Echelon, #P-5008), inositol 1,5-bisphosphate [Ins(1,5)P2; Echelon, #Q-0015], 1,2-dioleoyl-*sn*-glycero-3-phospho-(1′-myo-inositol-5′-phosphate) (di-C 18:1 PI5P; Avanti Polar Lipids, #850152P), 1-heptadecanoyl-2-(5Z,8Z,11Z,14Z-eicosatetraenoyl)-*sn*-glycero-3-phospho-(1′-myo-inositol-5′-phosphate) (17:0,20:4 PI5P; Avanti Polar Lipids, #LM1902), 1,2-dipalmitoyl-*sn*-glycero-3-phosphoethanolamine-*N*-(biotinyl) (sodium salt) (di-C 16:0 biotinyl PE; Avanti Polar Lipids, #870285), 1,2-dimyristoyl-*sn*-glycero-3-phosphoethanolamine (di-C 14:0 PE; Avanti Polar Lipids, #850745), 1,2-dioleoyl-*sn*-glycero-3-phosphoethanolamine-*N*-(biotinyl) (sodium salt) (di-C 18:1 biotinyl PE; Avanti Polar Lipids, #870282), 1,2-distearoyl-*sn*-glycero-3-phosphoethanolamine-*N*-[methoxy(polyethylene glycol)-550] (ammonium salt) (di-C 18:0 PEG550PE; Avanti Polar Lipids, #880520), cholesterol-(polyethylene glycol-600) (Avanti Polar Lipids, #880001), 1,2-dipalmitoyl-*sn*-glycero-3-phosphate (di-C 16:0 PA; Avanti Polar Lipids, #830855), 1,2-dimyristoyl-*sn*-glycero-3-phosphocholine (DMPC) (Anatrace, #D514), and 1,2-diheptanoyl-*sn*-glycero-3-phosphocholine (DHPC) (Anatrace, #D607).

Peptides

The following peptides were custom synthesized and purified to >90% by Synpeptide Co: H3unmodified (1 to 20 amino acids) = ARTKQTARKSTGGKAPRKQL-K(biotin), H3K9me3 (1 to 20 amino acids) = ARTKQTARK(me3)STGGKAPRKQL-K(biotin), human LIG1

(118 to 128 amino acids) = IPKRRTARKQL-K(biotin), LIG1me3 (118 to 128 amino acids) = IPKRRTARK(me3)QL-K(biotin), hUHRF1 linker 2 (286 to 306 amino acids) = GSPMVDNPMRRKSGPSCK-HC-K(biotin), and hUHRF1 linker 2 (286 to 306 amino acids) R296A = GSPMVDNPMRAKSGPSCKHC-K(biotin). H3(1-20)K9me3-thioester was obtained from Charité Universitätsmedizin Berlin, Institut für Biochemie, P. Henklein: ARTKQTARK(me3)STGGKAPRKQL-(4-mercaptophenylacetic acid)thioester.

Protein expression and purification

Proteins were expressed in BL21-DE3 RIL *Escherichia coli* cells. Bacterial cultures growing at 30°C with shaking were induced with 0.75 mM isopropyl-β-D-thiogalactopyranoside at OD_{600} (optical density at 600 nm) of 0.5 and 0.6. After continued growth at 25°C for 3 hours, cells were harvested and lysed. His-tagged proteins were purified on HisPur Ni-NTA resin (Thermo Fisher Scientific) according to the manufacturer's protocols. Eluates were dialyzed against 50 mM tris-HCl (pH 8.0), 150 mM NaCl, 10% (v/v) glycerol, and 1 mM dithiothreitol (DTT). Proteins were stored at 4°C until further use.

Microscale thermophoresis

C-terminally His6-tagged proteins were labeled using the Monolith His-tag labeling kit RED-tris-NTA (Nanotemper #MO-L008) following the manufacturer's protocol. Briefly, 400 nM protein was incubated with 100 nM His-tag labeling dye in MST buffer [20 mM Hepes-NaOH (pH 7.9), 150 mM NaCl, 0.05% (v/v) Tween 20] for 30 min at room temperature. Labeled proteins were cleared by centrifugation at 15,000*g* for 10 min at 4°C.

Fluorophore-labeled protein was incubated with various ligands at room temperature for 15 min before measuring on a Monolith NT.115 instrument (NanoTemper, 80% light-emitting diode power, 40% MST power). For competition assays, protein-DNA or protein-PIP concentrations were kept constant. Data points were fitted using the following equation

$$[AL] = ½^{*}(([A_0]+[L_0]+K_d)-(([A_0]+[L_0]+K_d)^2 - 4^{*}[A_0]^{*}[L_0])^{1/2})$$

where K_d is the dissociation constant; $[A_0]$, concentration of fluorescent molecule; $[L_0]$, concentration of ligand/ binding partner; and $[AL]$, concentration of the complex of *A* and *L*. All binding measurements were performed in triplicate as biological and technical replicates with at least two independent protein preparations.

Peptide pull down

A total of 40 µl of streptavidin paramagnetic beads (MagneSphere, Promega) was washed three times with phosphate-buffered saline (PBS) in low-binding tubes. A total of 10 µg of biotin-labeled hUHRF1 linker 2 peptides or water was added for 1 hour at room temperature with rotation, followed by three washes with PBS. A total of 10 µg of recombinant hUHRF1 linker 4 peptide in 500 µl of binding buffer [20 mM Hepes-NaOH (pH 7.9), 150 mM NaCl, 0.05% (v/v) Tween 20] was added, and reactions were incubated for 1 hour at room temperature with rotation in the absence and presence of 10-fold molar excess of di-C 16:0 PI5P or di-C 16:0 PI3P (final concentrations, 2.15 µM linker 4 and 21.5 µM PIP). Beads were washed three times with binding buffer, and the recovered material was eluted in 30 µl of PDelute buffer [50 mM tris-HCl (pH 8.0), 25% (v/v) glycerol, 0.25% (w/v) bromophenol blue, 1 mM EDTA, 2% (w/v) SDS, 1 mM TCEP (Tris(2-carboxyethyl)phosphine)] by boiling for 5 min.

Nucleosome reconstitution

Unmodified and H3K9me3 mononucleosomes were reconstituted as described previously (*71*). Briefly, recombinant *Xenopus laevis* core histones were expressed and purified in bacteria. Histone H3 carrying the K9me3 modification was obtained by ligating an H3(1 to 20) K9me3-thioester peptide to H3Δ(1-20)A21C using native protein ligation. Reconstituted histone octamers were dialyzed onto 147–base pair Widom 601 DNA obtained by polymerase chain reaction amplification and incorporating a biotinylated oligonucleotide at the 5′-end (5′ biotin-CTGGAGAATCCCGGTGCCGAGGC 3′.

Nucleosome pull down

A total of 40 µl of streptavidin paramagnetic beads (MagneSphere, Promega) was washed three times with PD300 buffer [20 mM Hepes-NaOH (pH 7.9), 300 mM KCl, 0.2% (v/v) Tween 20, and 20% (v/v) glycerol]. A total of 2 µg biotin-labeled mononucleosomes or water was added for overnight incubation at 4°C with rotation, followed by three washes with PD300. Recombinant proteins were incubated in the absence and presence of 10-fold molar excess of di-C 16:0 PI5P or di-C 16:0 PI4P overnight at 4°C. A total of 10 µg recombinant proteins (without and with PIPs) in 500 µl of binding buffer was added to washed beads, and reactions were incubated for 3 hours at 4°C with rotation. Beads were washed six times with PD300, and the recovered material was eluted in 30 µl of PDelute buffer [50 mM tris-HCl (pH 8), 25% (v/v) glycerol, 0.25% (w/v) bromophenol blue, 1 mM EDTA, 2% (w/v) SDS, and 1 mM TCEP] by boiling for 10 min. The intensity of the hUHRF1 band was integrated for each reaction using ImageJ (http://imagej.nih.gov/ij/). Values were corrected for mock and normalized to the intensity of the H2A/H2B band. Fold change was determined as ratio of H3K9me3/H3unmodified normalized signal. Experiments were performed with three technical replicates using two independently prepared samples.

Electrophoretic mobility shift assay

Recombinant proteins were incubated in the absence and presence of 10-fold molar excess of di-C 16:0 PI5P or di-C 16:0 PI4P overnight at 4°C. A total of 0.4 pmol of mononucleosomes was titrated with increasing amounts (up to 200-fold molar excess) of recombinant proteins for 10 min on ice in EMSA buffer [20 mM Hepes-NaOH (pH 7.9), 150 mM NaCl, 0.25% (v/v) Tween 20] and a total volume of 10 µl. Reactions were run on 1% agarose gels in 0.2× TBE after adding 2% (v/v) glycerol [4°C for 90 min at 100 V, stained for 15 min with ethidium bromide (0.5 µg/µl) in TE buffer].

Binding of hUHRF1 to mononucleosomes was quantified as previously described (*24*). The intensity of the band corresponding to the unbound nucleosome was integrated for each reaction using ImageJ (http://imagej.nih.gov/ij/). Values obtained for reactions containing hUHRF1 were normalized to the value of the nucleosome-only control reaction. Two fully independent experiments (biological replicates) and quantifications were performed, and the averaged values were plotted using GraphPad Prism. The apparent K_d was derived from the hUHRF1 concentration yielding 50% binding saturation.

HDXMS measurements and analysis

hUHRF1 and H3 peptides or hUHRF1(PI5P/ PI3P) were mixed at final concentrations of 1, 10, and 16.8 µM in buffer containing 50 mM tris-HCl (pH 7.9), 150 mM NaCl, and 1 mM DTT and incubated for 30 min at room temperature to allow complex formation. Deuterium on-exchange was carried out at 4°C by mixing 5 µl of each sample

with 15 µl of deuterium on-exchange buffer [10 mM tris-HCl [poteential of deuterium (pD) 8.3], 150 mM NaCl, in D_2O] yielding a final D_2O concentration of 75%. pD values for deuterium-based buffers were calculated as pD = pH + 0.4138. Upon mixing with on-exchange buffer, the amide protons are replaced over time with deuterons yielding an increased peptide mass. To quench the deuterium exchange reaction, samples (20 µl) were mixed with 30 µl of ice-cold quenched buffer [500 mM guanidine hydrochloride, 10% (v/v) glycerol, and 0.8% (v/v) formic acid, for a final pH of 2.4]. Samples were rapidly frozen in liquid nitrogen and stored at −80°C until further use. All HDXMS analyses were performed with three independent biological replicates.

For MS analysis, each sample (50 µl) was thawed on ice and loaded onto an in-house packed pepsin column for digestion. To this end, pepsin (Sigma-Aldrich) was coupled to POROS 20 AL support (Applied Biosystems), and the immobilized pepsin was packed into a column housing (2 mm by 2 cm, Upchurch). Pepsin-digested peptides were captured on a TARGA C8 5-µm Piccolo HPLC column (1.0 × 5.0 mm, Higgins Analytical) and eluted through an analytical C18 HPLC column (0.3 × 75 mm, Agilent) by a shaped 12 to 100% buffer B gradient at 6 µl/min (buffer A: 0.1% formic acid and buffer B: 0.1% formic acid and 99.9% acetonitrile). Eluting peptides were electrosprayed into the mass spectrometers (Exactive Plus EMR-Orbritrap or Q Exactive HF, both Thermo Fisher Scientific). Data were recorded using Xcalibur software (Thermo Fisher Scientific). MS-only data were acquired for the time course analysis. MS/MS data were collected in data-dependent mode to sequence hUHRF1 peptides resulting from pepsin digestion. Peptides were identified by database searching using SEQUEST (Bioworks v3.3.1 and Proteome Discoverer v2.4, Thermo Fisher Scientific) with a peptide tolerance of 8 parts per million and a fragment tolerance of 0.1 AMU (atomic mass unit).

A MATLAB-based program, ExMS2, was used to prepare the pool of peptides based on SEQUEST output files. EXMS2 (for hUHRF1-H3 peptides ± PI5P measurements) and HDExaminer software [for hUHRF1(PI5P/PI3P) measurements] were used to process and analyze the HDXMS data. The software identifies the peptide envelope centroid values for nondeuterated as well as deuterated peptides and uses the information to calculate the level of peptide deuteration for each peptide at every time point. Individual deuterated peptides were corrected for loss of deuterium label during HDXMS data collection by normalizing to the maximal deuteration level of each peptide [measured in a "fully deuterated" (FD) reference sample]. The FD sample was prepared in 75% deuterium to mimic the exchange experiment but under acidic denaturing conditions (0.5% formic acid) and incubated over 48 hours to allow each amide proton position along the entire polypeptide to undergo full exchange. The software automatically performs the correction when provided with the FD file. For each peptide, we compared the extent of deuteration as measured in the FD sample to the theoretical maximal deuteration (i.e., if no back exchange occurs). The median extent of back exchange in our experiments was between 25 and 26% (fig. S8). HDX data tables of our analysis were included in table S4 as described in (*72*).

NMR spectroscopy

All NMR spectra were acquired on Bruker Avance NEO NMR spectrometers operating at 700, 800, and 950 MHz equipped with sensitive triple resonance TCI cryoprobes. NMR samples for the backbone assignment of 200 µM uniformly ^{15}N,^{13}C-double–labeled linker 4 (hUHRF1 amino acids 605 to 675-6xHIS) were prepared in 50 mM tris-HCl (pH 6.5), 150 mM NaCl, 90%/10% (v/v) H_2O/D_2O, and 1 mM DTT. Complete sequence-specific backbone resonance assignment of linker 4 was obtained at 15°C from 3D triple-resonance HSQC-based HNCACB, CBCA(CO)NH, HNCA, HN(CO)CA, HN(CA)CO, and HNCO spectra (https://pubs.acs.org/doi/abs/10.1021/bi00471a022). Spectra were processed in Topspin 4.0.7 and analyzed in CARA (http://cara.nmr-software.org/). The side-chain chemical shifts were assigned on the basis of the following experiments: heteronuclear 2D ^{1}H-^{13}C HSQC and 3D C(CO)NH, 3D (H)CCH-TOCSY, and H(C)CH-TOCSY (mixing time of 16.2 ms) and 3D ^{13}C-edited HSQC-NOESY (mixing time of 100 ms) covering the aliphatic region. The titrations with phospholipids and with linker 2 were monitored with 2D ^{1}H-^{13}C HSQC spectra at 25°C recorded on 20 µM uniformly ^{15}N,^{13}C–labeled linker 4 in 50 mM tris-HCl (pH 7.9) and 150 mM NaCl 1 mM DTT with 10-fold molar excess of ligand (PI5P, PI4P, or linker). Titration was performed using two independently prepared linker 4 samples.

Bicelle formation and analysis

di-C 16:0 PI5P/DMPC/DHPC and di-C 16:0 PI5P/DHPC bicelles at 0.4 molar ratio of lipids were produced as described (*73*). DMPC, DHPC, and di-C 16:0 PI5P were dissolved in water. The slurries were vortexed and sonicated until the material was fully dissolved. di-C 16:0 PI5P (250 µM), DMPC (250 µM), and DHPC (1 mM) were mixed to obtain a sample with a total lipid ([PC] ≡ [PI5P + DMPC] + [DHPC]) concentration of 1.5 mM. di-C 16:0 PI5P/DHPC bicelles were prepared by mixing 500 µM PI5P with 1 mM DHPC. This mixture was subjected to several cycles of gentle heating to 42°C combined with vortexing until a clear nonviscous solution was obtained. Bicelles were incubated on ice for 15 min in 20 mM Hepes-NaOH (pH 7.9) and 150 mM NaCl at a concentration of 150 µM. A total of 4 µl of sample was added to a continuous carbon grid after glow discharge (Solarus, Gatan). After 1-min incubation, samples were blotted with filter paper and stained three times with 2% (w/v) uranyl formate. The stain was removed by blotting with filter paper, and the grids were dried at room temperature before imaging on a Thermo Fisher Scientific Tecnai Twin microscope (Gatan UltraScan 4000, 120 keV with a 4k × 4k charge-coupled device camera).

SUPPLEMENTARY MATERIALS

Supplementary material for this article is available at https://science.org/doi/10.1126/sciadv.abl9461

View/request a protocol for this paper from *Bio-protocol*.

REFERENCES AND NOTES

1. H. Xie, S. Vucetic, L. M. Iakoucheva, C. J. Oldfield, A. K. Dunker, V. N. Uversky, Z. Obradovic, Functional anthology of intrinsic disorder. 1. Biological processes and functions of proteins with long disordered regions. *J. Proteome Res.* **6**, 1882–1898 (2007).
2. S. Vucetic, H. Xie, L. M. Iakoucheva, C. J. Oldfield, A. K. Dunker, Z. Obradovic, V. N. Uversky, Functional anthology of intrinsic disorder. 2. Cellular components, domains, technical terms, developmental processes, and coding sequence diversities correlated with long disordered regions. *J. Proteome Res.* **6**, 1899–1916 (2007).
3. Y. Stijf-Bultsma, L. Sommer, M. Tauber, M. Bamino acidslbaki, P. Giardoglou, D. R. Jones, K. A. Gelato, J. van Pelt, Z. Shah, H. Rahnamoun, C. Toma, K. E. Anderson, P. Hawkins, S. M. Lauberth, A.-P. G. Haramis, D. Hart, W. Fischle, N. Divecha, The basal transcription complex component TAF3 transduces changes in nuclear phosphoinositides into transcriptional output. *Mol. Cell* **58**, 453–467 (2015).
4. B. L. Hamann, R. D. Blind, Nuclear phosphoinositide regulation of chromatin. *J. Cell. Physiol.* **233**, 107–123 (2018).
5. K. Zhao, W. Wang, O. J. Rando, Y. Xue, K. Swiderek, A. Kuo, G. R. Crabtree, Rapid and phosphoinositol-dependent binding of the SWI/SNF-like BAF complex to chromatin after T lymphocyte receptor signaling. *Cell* **95**, 625–636 (1998).

6. L. Gapa, H. Alfardus, W. Fischle, Unconventional metabolites in chromatin regulation. *Biosci. Rep.* **42**, (2022).
7. C. T. Szlenk, J. B. Gc, S. Natesan, Does the lipid bilayer orchestrate access and binding of ligands to transmembrane orthosteric/allosteric sites of G protein-coupled receptors? *Mol. Pharmacol.* **96**, 527–541 (2019).
8. Z. Cournia, A. Chatzigoulas, Allostery in membrane proteins. *Curr. Opin. Struct. Biol.* **62**, 197–204 (2020).
9. R. G. Jacobsen, F. Mazloumi Gavgani, A. J. Edson, M. Goris, A. Altankhuyag, A. E. Lewis, Polyphosphoinositides in the nucleus: Roadmap of their effectors and mechanisms of interaction. *Adv. Biol. Regul.* **72**, 7–21 (2019).
10. I. N. Krylova, E. P. Sablin, J. Moore, R. X. Xu, G. M. Waitt, J. A. MacKay, D. Juzumiene, J. M. Bynum, K. Madauss, V. Montana, L. Lebedeva, M. Suzawa, J. D. Williams, S. P. Williams, R. K. Guy, J. W. Thornton, R. J. Fletterick, T. M. Willson, H. A. Ingraham, Structural analyses reveal phosphatidyl inositols as ligands for the NR5 orphan receptors SF-1 and LRH-1. *Cell* **120**, 343–355 (2005).
11. H. Yu, K. Fukami, Y. Watanabe, C. Ozaki, T. Takenawa, Phosphatidylinositol 4,5-bisphosphate reverses the inhibition of RNA transcription caused by histone H1. *Eur. J. Biochem.* **251**, 281–287 (1998).
12. O. Gozani, P. Karuman, D. Jones, D. Ivanov, J. Cha, A. Lugovskoy, C. Baird, H. Zhu, S. Field, S. Lessnick, J. Villasenor, B. Mehrotra, J. Chen, V. Rao, J. Brugge, C. Ferguson, B. Payrastre, D. Myszka, L. Cantley, J. Yuan, The PHD finger of the chromatin-associated protein ING2 functions as a nuclear phosphoinositide receptor. *Cell* **114**, 99–111 (2003).
13. M. W. Bunce, I. V. Boronenkov, R. A. Anderson, Coordinated activation of the nuclear ubiquitin ligase Cul3-SPOP by the generation of phosphatidylinositol 5-phosphate*. *J. Biol. Chem.* **283**, 8678–8686 (2008).
14. K. A. Gelato, M. Tauber, M. S. Ong, S. Winter, K. Hiragami-Hamada, J. Sindlinger, A. Lemak, Y. Bultsma, S. Houliston, D. Schwarzer, N. Divecha, C. H. Arrowsmith, W. Fischle, Accessibility of different histone H3-binding domains of UHRF1 is allosterically regulated by phosphatidylinositol 5-phosphate. *Mol. Cell* **54**, 905–919 (2014).
15. J. Sharif, M. Muto, S. Takebayashi, I. Suetake, A. Iwamatsu, T. A. Endo, J. Shinga, Y. Mizutani-Koseki, T. Toyoda, K. Okamura, S. Tajima, K. Mitsuya, M. Okano, H. Koseki, The SRA protein Np95 mediates epigenetic inheritance by recruiting Dnmt1 to methylated DNA. *Nature* **450**, 908–912 (2007).
16. S. Maenohara, M. Unoki, H. Toh, H. Ohishi, J. Sharif, H. Koseki, H. Sasaki, Role of UHRF1 in de novo DNA methylation in oocytes and maintenance methylation in preimplantation embryos. *PLOS Genet.* **13**, e1007042 (2017).
17. M. Mancini, E. Magnani, F. Macchi, I. M. Bonapace, The multi-functionality of UHRF1: Epigenome maintenance and preservation of genome integrity. *Nucleic Acids Res.* **49**, 6053–6068 (2021).
18. Y. Tian, M. Paramasivam, G. Ghosal, D. Chen, X. Shen, Y. Huang, S. Akhter, R. Legerski, J. Chen, M. M. Seidman, J. Qin, L. Li, UHRF1 contributes to DNA damage repair as a lesion recognition factor and nuclease scaffold. *Cell Rep.* **10**, 1957–1966 (2015).
19. C. Bronner, G. Fuhrmann, F. L. Chédin, M. Macaluso, S. Dhe-Paganon, UHRF1 links the histone code and DNA methylation to ensure faithful epigenetic memory inheritance. *Genet. Epigenet.* **2009**, 29–36 (2010).
20. M. Bostick, J. K. Kim, P.-O. Estève, A. Clark, S. Pradhan, S. E. Jacobsen, UHRF1 plays a role in maintaining DNA methylation in mammalian cells. *Science* **317**, 1760–1764 (2007).
21. Y. Yang, G. Liu, L. Qin, L. Ye, F. Zhu, Y. Ying, Overexpression of UHRF1 and its potential role in the development of invasive ductal breast cancer validated by integrative bioinformatics and immunohistochemistry analyses. *Transl. Cancer Res.* **8**, 1086–1096 (2019).
22. H. Zhuo, J. Tang, Z. Lin, R. Jiang, X. Zhang, J. Ji, P. Wang, B. Sun, The aberrant expression of MEG3 regulated by UHRF1 predicts the prognosis of hepatocellular carcinoma. *Mol. Carcinog.* **55**, 209–219 (2016).
23. L. Cui, J. Chen, Q. Zhang, X. Wang, J. Qu, J. Zhang, S. Dang, Up-regulation of UHRF1 by oncogenic Ras promoted the growth, migration, and metastasis of pancreatic cancer cells. *Mol. Cell. Biochem.* **400**, 223–232 (2015).
24. B. M. Foster, P. Stolz, C. B. Mulholland, A. Montoya, H. Kramer, S. Bultmann, T. Bartke, Critical role of the UBL domain in stimulating the E3 ubiquitin ligase activity of UHRF1 toward chromatin. *Mol. Cell* **72**, 739–752.e9 (2018).
25. P. A. DaRosa, J. S. Harrison, A. Zelter, T. N. Davis, P. Brzovic, B. Kuhlman, R. E. Klevit, A bifunctional role for the UHRF1 UBL domain in the control of hemi-methylated DNA-dependent histone ubiquitylation. *Mol. Cell* **72**, 753–765.e6 (2018).
26. N. Nady, A. Lemak, J. R. Walker, G. V. Avvakumov, M. S. Kareta, M. Achour, S. Xue, S. Duan, A. Allali-Hassani, X. Zuo, Y. X. Wang, C. Bronner, F. Chédin, C. H. Arrowsmith, S. Dhe-Paganon, Recognition of multivalent histone states associated with heterochromatin by UHRF1 protein. *J. Biol. Chem.* **286**, 24300–24311 (2011).
27. L. Hu, Z. Li, P. Wang, Y. Lin, Y. Xu, Crystal structure of PHD domain of UHRF1 and insights into recognition of unmodified histone H3 arginine residue 2. *Cell Res.* **21**, 1374–1378 (2011).
28. C. Wang, J. Shen, Z. Yang, P. Chen, B. Zhao, W. Hu, W. Lan, X. Tong, H. Wu, G. Li, C. Cao, Structural basis for site-specific reading of unmodified R2 of histone H3 tail by UHRF1 PHD finger. *Cell Res.* **21**, 1379–1382 (2011).
29. K. Arita, M. Ariyoshi, H. Tochio, Y. Nakamura, M. Shirakawa, Recognition of hemi-methylated DNA by the SRA protein UHRF1 by a base-flipping mechanism. *Nature* **455**, 818–821 (2008).
30. G. V. Avvakumov, J. R. Walker, S. Xue, Y. Li, S. Duan, C. Bronner, C. H. Arrowsmith, S. Dhe-Paganon, Structural basis for recognition of hemi-methylated DNA by the SRA domain of human UHRF1. *Nature* **455**, 822–825 (2008).
31. E. Citterio, R. Papait, F. Nicassio, M. Vecchi, P. Gomiero, R. Mantovani, P. P. Di Fiore, I. M. Bonapace, Np95 is a histone-binding protein endowed with ubiquitin ligase activity. *Mol. Cell. Biol.* **24**, 2526–2535 (2004).
32. Y. Jenkins, V. Markovtsov, W. Lang, P. Sharma, D. Pearsall, J. Warner, C. Franci, B. Huang, J. Huang, G. C. Yam, J. P. Vistan, E. Pali, J. Vialard, M. Janicot, J. B. Lorens, D. G. Payan, Y. Hitoshi, Critical role of the ubiquitin ligase activity of UHRF1, a nuclear RING finger protein, in tumor cell growth. *Mol. Biol. Cell* **16**, 5621–5629 (2005).
33. A. Nishiyama, L. Yamaguchi, J. Sharif, Y. Johmura, T. Kawamura, K. Nakanishi, S. Shimamura, K. Arita, T. Kodama, F. Ishikawa, H. Koseki, M. Nakanishi, Uhrf1-dependent H3K23 ubiquitylation couples maintenance DNA methylation and replication. *Nature* **502**, 249–253 (2013).
34. M. Tauber, W. Fischle, Conserved linker regions and their regulation determine multiple chromatin-binding modes of UHRF1. *Nucleus* **6**, 123–132 (2015).
35. M. Tauber, S. Kreuz, A. Lemak, P. Mandal, Z. Yerkesh, A. Veluchamy, B. Al-Gashgari, A. Aljahani, L. V. Cortés-Medina, D. Azhibek, L. Fan, M. S. Ong, S. Duan, S. Houliston, C. H. Arrowsmith, W. Fischle, Alternative splicing and allosteric regulation modulate the chromatin binding of UHRF1. *Nucleic Acids Res.* **48**, 7728–7747 (2020).
36. J. Fang, J. Cheng, J. Wang, Q. Zhang, M. Liu, R. Gong, P. Wang, X. Zhang, Y. Feng, W. Lan, Z. Gong, C. Tang, J. Wong, H. Yang, C. Cao, Y. Xu, Hemi-methylated DNA opens a closed conformation of UHRF1 to facilitate its histone recognition. *Nat. Commun.* **7**, 11197 (2016).
37. S. B. Rothbart, B. M. Dickson, M. S. Ong, K. Krajewski, S. Houliston, D. B. Kireev, C. H. Arrowsmith, B. D. Strahl, Multivalent histone engagement by the linked tandem Tudor and PHD domains of UHRF1 is required for the epigenetic inheritance of DNA methylation. *Genes Dev.* **27**, 1288–1298 (2013).
38. T. Li, L. Wang, Y. Du, S. Xie, X. Yang, F. Lian, Z. Zhou, C. Qian, Structural and mechanistic insights into UHRF1-mediated DNMT1 activation in the maintenance DNA methylation. *Nucleic Acids Res.* **46**, 3218–3231 (2018).
39. K. R. Vann, T. G. Kutateladze, Histone H3 dual ubiquitylation mediates maintenance DNA methylation. *Mol. Cell* **68**, 261–262 (2017).
40. J. S. Harrison, E. M. Cornett, D. Goldfarb, P. A. DaRosa, Z. M. Li, F. Yan, B. M. Dickson, A. H. Guo, D. V. Cantu, L. Kaustov, P. J. Brown, C. H. Arrowsmith, D. A. Erie, M. B. Major, R. E. Klevit, K. Krajewski, B. Kuhlman, B. D. Strahl, S. B. Rothbart, Hemi-methylated DNA regulates DNA methylation inheritance through allosteric activation of H3 ubiquitylation by UHRF1. *eLife* **5**, e17101 (2016).
41. D. R. Jones, I. B.-R. Ramirez, M. Lowe, N. Divecha, Measurement of phosphoinositides in the zebrafish *Danio rerio*. *Nat. Protoc.* **8**, 1058–1072 (2013).
42. D. Sarkes, L. E. Rameh, A novel HPLC-based approach makes possible the spatial characterization of cellular PtdIns5P and other phosphoinositides. *Biochem. J.* **428**, 375–384 (2010).
43. Z.-M. Zhang, S. B. Rothbart, D. F. Allison, Q. Cai, J. S. Harrison, L. Li, Y. Wang, B. D. Strahl, G. G. Wang, J. Song, An allosteric interaction links USP7 to deubiquitination and chromatin targeting of UHRF1. *Cell Rep.* **12**, 1400–1406 (2015).
44. J. M. Dawicki-McKenna, M.-F. Langelier, J. E. DeNizio, A. A. Riccio, C. D. Cao, K. R. Karch, M. McCauley, J. D. Steffen, B. E. Black, J. M. Pascal, PARP-1 activation requires local unfolding of an autoinhibitory domain. *Mol. Cell* **60**, 755–768 (2015).
45. L. Zandarashvili, M.-F. Langelier, U. K. Velagapudi, M. A. Hancock, J. D. Steffen, R. Billur, Z. M. Hannan, A. J. Wicks, D. B. Krastev, S. J. Pettitt, C. J. Lord, T. T. Talele, J. M. Pascal, B. E. Black, Structural basis for allosteric PARP-1 retention on DNA breaks. *Science* **368**, eamino acidsx6367 (2020).
46. A. J. Ruthenburg, H. Li, D. J. Patel, C. D. Allis, Multivalent engagement of chromatin modifications by linked binding modules. *Nat. Rev. Mol. Cell Biol.* **8**, 983–994 (2007).
47. J. Cheng, Y. Yang, J. Fang, J. Xiao, T. Zhu, F. Chen, P. Wang, Z. Li, H. Yang, Y. Xu, Structural insight into coordinated recognition of trimethylated histone H3 lysine 9 (H3K9me3) by the plant homeodomain (PHD) and tandem tudor domain (TTD) of UHRF1 (ubiquitin-like, containing PHD and RING finger domains, 1) protein. *J. Biol. Chem.* **288**, 1329–1339 (2013).
48. M. Conrad, The mutation buffering concept of biomolecular structure. *J. Biosci.* **8**, 669–679 (1985).
49. K. Arita, S. Isogai, T. Oda, M. Unoki, K. Sugita, N. Sekiyama, K. Kuwata, R. Hamamoto, H. Tochio, M. Sato, M. Ariyoshi, M. Shirakawa, Recognition of modification status on a histone H3 tail by linked histone reader modules of the epigenetic regulator UHRF1. *Proc. Natl. Acad. Sci. U.S.A.* **109**, 12950–12955 (2012).
50. L. Gao, X.-F. Tan, S. Zhang, T. Wu, Z.-M. Zhang, H.-W. Ai, J. Song, An intramolecular interaction of UHRF1 reveals dual control for its histone association. *Structure* **26**, 304–311.e3 (2018).

51. R. S. Houliston, A. Lemak, A. Iqbal, D. Ivanochko, S. Duan, L. Kaustov, M. S. Ong, L. Fan, G. Senisterra, P. J. Brown, Y. X. Wang, C. H. Arrowsmith, Conformational dynamics of the TTD-PHD histone reader module of the UHRF1 epigenetic regulator reveals multiple histone-binding states, allosteric regulation, and druggability. *J. Biol. Chem.* **292**, 20947–20959 (2017).
52. C. Qian, S. Li, J. Jakoncic, L. Zeng, M. J. Walsh, M. M. Zhou, Structure and hemimethylated CpG binding of the SRA domain from human UHRF1. *J. Biol. Chem.* **283**, 34490–34494 (2008).
53. M. Ghoneim, H. A. Fuchs, C. A. Musselman, Histone tail conformations: A fuzzy affair with DNA. *Trends Biochem. Sci.* **46**, 564–578 (2021).
54. L. Ferry, A. Fournier, T. Tsusaka, G. Adelmant, T. Shimazu, S. Matano, O. Kirsh, R. Amouroux, N. Dohmae, T. Suzuki, G. J. Filion, W. Deng, M. de Dieuleveult, L. Fritsch, S. Kudithipudi, A. Jeltsch, H. Leonhardt, P. Hajkova, J. A. Marto, K. Arita, Y. Shinkai, P. A. Defossez, Methylation of DNA ligase 1 by G9a/GLP recruits UHRF1 to replicating DNA and regulates DNA methylation. *Mol. Cell* **67**, 550–565.e5 (2017).
55. S. Kori, L. Ferry, S. Matano, T. Jimenji, N. Kodera, T. Tsusaka, R. Matsumura, T. Oda, M. Sato, N. Dohmae, T. Ando, Y. Shinkai, P.-A. Defossez, K. Arita, Structure of the UHRF1 tandem tudor domain bound to a methylated non-histone protein, LIG1, reveals rules for binding and regulation. *Structure* **27**, 485–496.e7 (2019).
56. J. A. Nunès, G. Guittard, An emerging role for PI5P in T cell biology. *Front. Immunol.* **4**, 80 (2013).
57. J. B. Morris, K. A. Hinchliffe, A. Ciruela, A. J. Letcher, R. F. Irvine, Thrombin stimulation of platelets causes an increase in phosphatidylinositol 5-phosphate revealed by mass assay. *FEBS Lett.* **475**, 57–60 (2000).
58. J. Viaud, F. Lagarrigue, D. Ramel, S. Allart, G. Chicanne, L. Ceccato, D. Courilleau, J. M. Xuereb, O. Pertz, B. Payrastre, F. Gaits-Iacovoni, Phosphatidylinositol 5-phosphate regulates invasion through binding and activation of Tiam1. *Nat. Commun.* **5**, 4080 (2014).
59. T. Kawasaki, N. Takemura, D. M. Standley, S. Akira, T. Kawai, The second messenger phosphatidylinositol-5-phosphate facilitates antiviral innate immune signaling. *Cell Host Microbe* **14**, 148–158 (2013).
60. A. Poli, A. E. Zaurito, S. Abdul-Hamid, R. Fiume, I. Faenza, N. Divecha, Phosphatidylinositol 5 phosphate (PI5P): From behind the scenes to the front (nuclear) stage. *Int. J. Mol. Sci.* **20**, 2080 (2019).
61. M. Chen, T. Wen, H. T. Horn, V. K. Chandrahas, N. Thapa, S. Choi, V. L. Cryns, R. A. Anderson, The nuclear phosphoinositide response to stress. *Cell Cycle* **19**, 268–289 (2020).
62. M. Achour, G. Fuhrmann, M. Alhosin, P. Rondé, T. Chataigneau, M. Mousli, V. B. Schini-Kerth, C. Bronner, UHRF1 recruits the histone acetyltransferase Tip60 and controls its expression and activity. *Biochem. Biophys. Res. Commun.* **390**, 523–528 (2009).
63. H. Mistry, L. Gibson, J. W. Yun, H. Sarras, L. Tamblyn, J. P. McPherson, Interplay between Np95 and Eme1 in the DNA damage response. *Biochem. Biophys. Res. Commun.* **375**, 321–325 (2008).
64. M. De Vos, R. El Ramy, D. Quénet, P. Wolf, F. Spada, N. Magroun, F. Babbio, V. Schreiber, H. Leonhardt, I. M. Bonapace, F. Dantzer, Poly(ADP-ribose) polymerase 1 (PARP1) associates with E3 ubiquitin-protein ligase UHRF1 and modulates UHRF1 biological functions*. *J. Biol. Chem.* **289**, 16223–16238 (2014).
65. Y. Xu, C. Xu, B. D. Price, Chapter 10 - mechanistic links between ATM and histone methylation codes during DNA repair, in *Progress in Molecular Biology and Translational Science*, P. W. Doetsch, Ed. (Academic Press, 2012), vol. 110, pp. 263–288.
66. X. Ming, Z. Zhang, Z. Zou, C. Lv, Q. Dong, Q. He, Y. Yi, Y. Li, H. Wang, B. Zhu, Kinetics and mechanisms of mitotic inheritance of DNA methylation and their roles in aging-associated methylome deterioration. *Cell Res.* **30**, 980–996 (2020).
67. R. Fiume, I. Faenza, B. Sheth, A. Poli, M. C. Vidalle, C. Mazzetti, S. H. Abdul, F. Campagnoli, M. Fabbrini, S. T. Kimber, G. A. Mariani, J. Xian, M. V. Marvi, S. Mongiorgi, Z. Shah, N. Divecha, Nuclear phosphoinositides: Their regulation and roles in nuclear functions. *Int. J. Mol. Sci.* **20**, 2991 (2019).
68. A. M. Joffrin, A. M. Saunders, D. Barneda, V. Flemington, A. L. Thompson, H. J. Sanganee, S. J. Conway, Development of isotope-enriched phosphatidylinositol-4- and 5-phosphate cellular mass spectrometry probes. *Chem. Sci.* **12**, 2549–2557 (2021).
69. A. Meister, M. Gabi, P. Behr, P. Studer, J. Vörös, P. Niedermann, J. Bitterli, J. Polesel-Maris, M. Liley, H. Heinzelmann, T. Zambelli, FluidFM: Combining atomic force microscopy and nanofluidics in a universal liquid delivery system for single cell applications and beyond. *Nano Lett.* **9**, 2501–2507 (2009).
70. O. Guillaume-Gentil, E. Potthoff, D. Ossola, P. Dörig, T. Zambelli, J. A. Vorholt, Force-controlled fluidic injection into single cell nuclei. *Small* **9**, 1904–1907 (2013).
71. K. Hiragami-Hamada, S. Soeroes, M. Nikolov, B. Wilkins, S. Kreuz, C. Chen, I. A. De La Rosa-Velázquez, H. M. Zenn, N. Kost, W. Pohl, A. Chernev, D. Schwarzer, T. Jenuwein, M. Lorincz, B. Zimmermann, P. J. Walla, H. Neumann, T. Baubec, H. Urlaub, W. Fischle, Dynamic and flexible H3K9me3 bridging via HP1β dimerization establishes a plastic state of condensed chromatin. *Nat. Commun.* **7**, 11310 (2016).
72. G. R. Masson, J. E. Burke, N. G. Ahn, G. S. Anand, C. Borchers, S. Brier, G. M. Bou-Assaf, J. R. Engen, S. W. Englander, J. Faber, R. Garlish, P. R. Griffin, M. L. Gross, M. Guttman, Y. Hamuro, A. J. R. Heck, D. Houde, R. E. Iacob, T. J. D. Jørgensen, I. A. Kaltashov, J. P. Klinman, L. Konermann, P. Man, L. Mayne, B. D. Pascal, D. Reichmann, M. Skehel, J. Snijder, T. S. Strutzenberg, E. S. Underbakke, C. Wagner, T. E. Wales, B. T. Walters, D. D. Weis, D. J. Wilson, P. L. Wintrode, Z. Zhang, J. Zheng, D. C. Schriemer, K. D. Rand, Recommendations for performing, interpreting and reporting hydrogen deuterium exchange mass spectrometry (HDX-MS) experiments. *Nat. Methods* **16**, 595–602 (2019).
73. J. Björnerås, M. Nilsson, L. Mäler, Analysing DHPC/DMPC bicelles by diffusion NMR and multivariate decomposition. *Biochim. Biophys. Acta Biomembr.* **1848**, 2910–2917 (2015).

Acknowledgments: We thank A. Aljahani for help with MST assays, S. Kreuz for scientific input during this study, and members of the Fischle laboratory for discussions. **Funding:** This work was supported by the King Abdullah University of Science and Technology (intramural funds and award OSR-2015-CRG-2616 of the KAUST Office of Sponsored Research to W.F.) and NIH grants R35GM130302 (to B.E.B.) and F32GM128265 (to L.Z.). **Author contributions:** P.M. and W.F. conceived and designed the project. P.M. performed all sample preparation and did most of the quantitative measurements. K.E. performed all nucleosome-related binding experiments and analyzed the data. Z.Y. prepared recombinant nucleosomes, performed some binding assays, and provided negative staining of lipid bicelles. V.K. and K.S. measured and analyzed NMR spectra. Ł.J. directed the NMR part of the work. B.E.B. designed, contributed to, and supervised HDXMS experiments. P.M., L.Z., and D.B. performed HDXMS measurements. P.M. analyzed the HDXMS data. W.F. supervised the course of the study. P.M. and W.F. wrote the manuscript. All authors discussed the results and commented on the manuscript. **Competing interests:** The authors declare that they have no competing interests. **Data and materials availability:** All data needed to evaluate the conclusions in the paper are present in the paper and/or the Supplementary Materials. No custom computer code was used in this study.

Submitted 15 August 2021
Accepted 11 July 2022
Published 24 August 2022
10.1126/sciadv.abl9461